

HERON contains contributions based mainly on research work performed in I.B.B.C. and STEVIN and related to strength of materials and structures and materials science.

## Contents

### THEORY AND EXPERIMENTS ON THE MECHANICAL BEHAVIOUR OF CRACKS IN PLAIN AND REINFORCED CONCRETE SUBJECTED TO SHEAR LOADING

*J. C. Walraven*  
*H. W. Reinhardt*

Dept. of Civil Engineering  
Delft University of Technology  
Stevinweg 1, Postbus 5048  
2600 GA Delft, The Netherlands

#### Jointly edited by:

STEVIN-LABORATORY  
of the Department of  
Civil Engineering of the  
Delft University of Technology,  
Delft, The Netherlands  
and  
I.B.B.C. INSTITUTE TNO  
for Building Materials  
and Building Structures,  
Rijswijk (ZH), The Netherlands.

#### EDITORIAL BOARD:

J. Witteveen, *editor in chief*  
G. J. van Alphen  
M. Dragosavić  
H. W. Reinhardt  
A. C. W. M. Vrouwenvelder  
L. van Zetten

#### Secretary:

G. J. van Alphen  
Stevinweg 1  
P.O. Box 5048  
2600 GA Delft, The Netherlands  
Tel. 0031-15-785919  
Telex 38070 BITHD

<b>Preface</b> .....	3
<b>Summary</b> .....	5
<b>1 Introduction</b> .....	7
<b>2 Information from the literature</b> .....	8
<b>3 Experimental investigation</b> .....	9
3.1 General remarks .....	9
3.2 Scope .....	10
3.2.1 Variables of tests with embedded bars	10
3.2.2 Variables of tests with external restraint bars .....	11
3.3 Specimens .....	11
3.3.1 Specimens with embedded bars .....	12
3.3.2 Specimens with external restraint bars	13
3.4 Testing arrangement and instrumentation .....	14
3.5 Testing procedure .....	15
3.6 Survey of experiments .....	15
3.6.1 Tests with embedded bars .....	15
3.6.2 Tests with external restraint bars .....	16
<b>4 Results of tests with embedded bars</b> .....	16
4.1 Tests with completely embedded bars	16
4.2 Tests with bars with interrupted bond	21
<b>5 Results of tests with external restraint bars</b> .....	22



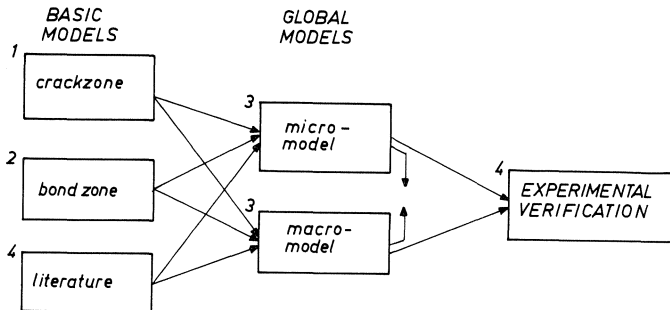
*This publication has been issued in close co-operation with the Netherlands Committee for Research, Codes and Specifications for Concrete (CUR-VB).*

<b>6 Basic analysis of aggregate interlock</b> .....	26
6.1 Fundamentals.....	26
6.2 Comparison between theory and experiments .....	33
6.3 Further analysis of aggregate interlock	35
<b>7 Analysis of the results of the tests with embedded bars</b> .....	40
7.1 General.....	40
7.2 Components involved in the transmission of forces.....	41
7.3 Analysis of test results .....	44
<b>8 A model for the behaviour of cracked reinforced concrete</b> .....	47
8.1 The stress-displacement relation for a single crack.....	47
8.2 The relation between stresses and displacements in cracked reinforced concrete.....	49
<b>9 Conclusions</b> .....	56
<b>10 Notations</b> .....	57
<b>11 References</b> .....	58
<b>12 Appendices</b> .....	63
12.1 Composition of the concrete mixtures used in the experiments .....	63
12.2 Stress-strain diagrams of the stirrup reinforcing steel.....	65
12.3 Loading arrangement used for the tests	66
12.4 Tests on specimens with embedded bars .....	67
12.4.1 Reinforcement normal to the crack...	67
12.4.2 Reinforcement inclined to the crack plane .....	68
12.5 Tests on specimens with external bars	68

Publications in HERON since 1970

## Preface

This issue of HERON contains the theoretical and experimental results of the research project "Shear transfer across cracks in concrete" which has been carried out in the Stevin Laboratory of Delft University of Technology. This project is part of the joint project "Betonmechanica" (concrete mechanics) which is being conducted by Rijkswaterstaat (State Public Works), TNO-IBBC (Institute TNO for Building Materials and Building Structures) and the two Universities of Technology at Eindhoven and Delft, respectively. The whole project is outlined in the following diagram showing the sub-projects and their interrelations.



The present report deals with theoretical and experimental studies concerning the behaviour of the cracked zone, whereas the other topics will be dealt with in the HERON issues 1<sub>B</sub> and 1<sub>C</sub> of this volume.

The joint project is being supervised and partly financed by the CUR-VB (Netherlands Committee for Research, Codes and Specifications for Concrete), which has set up the working committee A 26 "Betonmechanica". The members of this committee are prof. ir. B. W. van der Vlugt (chairman), prof. dr. ir. J. Blaauwendraad (secretary), prof. ir. A. L. Bouma, prof. dr. ir. A. S. G. Bruggeling, prof. ir. J. W. Kamerling, prof. ir. H. Lambotte, prof. Dr.-Ing. G. Mehlhorn, ir. Th. Monnier, prof. Dr.-Ing. H. W. Reinhardt, ing. A. C. van Riel, ir. J. C. Slagter (mentor), prof. ir. J. Witteveen, prof. Dr. F. H. Wittmann. The authors are indebted to these persons for their contributions, help and encouragement.

Much of the experimental investigation work was done by Ir. E. Vos. The authors would like to thank him for his ideas and assistance.

This publication can be regarded as a comprehensive summary of all the results. A detailed account of the investigations is given in the following reports:

WALRAVEN, J. C., Mechanics of shear transfer in cracks in concrete – A survey of literature, Report No. 5-78-12, December 1978, Stevin Laboratory, Delft University of Technology.

WALRAVEN, J. C., E. VOS and H. W. REINHARDT, Experiments on shear transfer in cracks in concrete. Part I: Description of results, Report No. 5-79-3, January 1979, Stevin Laboratory, Delft University of Technology.

WALRAVEN, J. C., Experiments on shear transfer in cracks in concrete. Part II: Analysis of results, Report No. 5-79-10, November 1979, Stevin Laboratory, Delft University of Technology.

WALRAVEN, J. C., Aggregate interlock; A theoretical and experimental analysis, Doctoral thesis, October 1980, Delft University of Technology.

## THEORY AND EXPERIMENTS ON THE MECHANICAL BEHAVIOUR OF CRACKS IN PLAIN AND REINFORCED CONCRETE SUBJECTED TO SHEAR LOADING

### Summary

As result of the increasing difficulties in structural design associated with the increase in scale and complexity of new structures and their loading conditions in recent years, added impetus has been given to the development of numerical calculation techniques. Above all, the non-linear finite element methods, which are still being refined, may become powerful tools in future design. These methods, however, can only show to full advantage if the material characteristics to be inserted are adequately known. One of the characteristics affected by lack of information concerns the mechanism of transmission of forces across cracks whose faces are subjected to shear displacements. This mechanism is achieved by interaction of several components: axial and transverse stiffness (dowel action) of the reinforcement and direct transfer of forces between the rough concrete crack faces, generally denoted by the term “aggregate interlock”.

Experimental research and the derivation of a theoretical model gave insight into this phenomenon. Tests were carried out on precracked shear specimens. Variables in the tests were: the type of reinforcement (embedded reinforcing bars, external restraint bars), the concrete strength ( $13 < f_{cc} < 60 \text{ N/mm}^2$ ), the type of the concrete (sand gravel concrete, lightweight concrete), the grading of the concrete (continuous, discontinuous), the scale of the concrete ( $D_{\max} = 16$  and  $32 \text{ mm}$ ) and the initial crack width. Measurements have been carried out for determining the shear force, the crack displacements and, for the specimens with external reinforcement, the force in the restraining bars.

To obtain more insight into the mechanism of aggregate interlock also a theoretical model was developed, which was subsequently compared with the experimental results. The theory is based on the assumption that concrete can be conceived as a “two-phase” material which is composed of a collection of aggregate particles with high strength and stiffness (phase I), and a matrix material consisting of hardened cement paste with fine sand with lower strength and stiffness (phase II).

A crack in this composite material generally intersects the matrix, but not the aggregate particles, because the contact layer between particles and matrix is of relatively low quality. The transmission of forces during shear displacement of the crack faces is effected via local contact areas between the particles protruding from one of the crack faces and the matrix in the opposite crack face. The interdependence between forces and displacements of the crack faces is closely related to the deformation of the matrix material. The most probable distribution and orientation of the contact areas were determined by a statistical analysis. For this analysis the aggregate particles were simplified to spheres, protruding for an arbitrary part of their diameter from one of the crack faces. The coefficient of friction between particles and matrix at overriding, and the stress at which plastic deformation of the matrix occurs, were used as “adjusting parameters” in the model. It was shown that the experimental results could be adequately de-

scribed by the theoretical model. By means of a parameter study carried out with the model, the mechanism of transmission of forces was further analysed, focusing on the role of the individual particle fractions, the scale of the aggregate particles and the influence of the grading curve. It was demonstrated that the behaviour of cracks subjected to cyclic loading, as known from the literature, can also be explained by the model.

For cracks with embedded reinforcement an additional aspect has been observed. It appeared that in this case limit crack opening directions exist, which cannot be exceeded. This is attributed to the fact that around deformed bars local reduction of the crack width occurs: this reduction is attended with high shear stiffness so that high stress concentrations occur. These concentrations can result in microcracking around the bars, activating an additional mechanism of shear transfer. If around the bars soft sleeves were secured to both sides of the crack over short lengths, the effect disappeared and behaviour similar to that of the specimens with external reinforcement was obtained.

# Theory and experiments on the mechanical behaviour of cracks in plain and reinforced concrete subjected to shear loading

## 1 Introduction

Finite element computer programs for the analysis of structures have been developed in such a way that they are not only suited for linear problems but also for physically and geometrically non-linear ones, and even structures with stable or unstable cracks can be analysed. Stress and strain under service load conditions can be calculated, extraordinary loading conditions such as earthquake, impact, explosion, high and low temperature can be treated. In spite of the wide applicability of the computer programs, the reliability of the calculations and the meaningfulness of the results rely upon the basic relations which are being used for the description of the material properties. In linear elastic problems the definition of Young's modulus and Poisson's ratio is sufficient; in plastic problems, a yield stress and a flow rule must be added. In the analysis of cracked structures the behaviour of a crack under various states of stress must be modelled.

Reinforced concrete belongs to the type of structures which are assumed to be cracked under service conditions. This assumption is due to the fact that plain concrete has a comparatively small fracture strain in tension and therefore will crack at low stresses. Once cracked, the reinforcement becomes active and takes over the forces from the concrete. Whereas in the case of bending the behaviour of reinforced concrete has been extensively investigated and the physical model generally accepted, there is still a lack of knowledge in the case of shear forces, especially when the concrete is cracked.

In order to analyse cracked reinforced concrete structures by means of finite element programs the behaviour of cracks under shear loads must be modelled. It is known that shear forces in cracks are transferred by a combination of aggregate interlock, dowel action and axial restraint stiffness of the reinforcement crossing the crack, but there is little knowledge concerning the interaction of these phenomena.

Qualitatively it is understood that, during shear motion of a crack, opening of the crack (dilatancy) due to the unevenness of the crack surfaces will also occur, and it has been pointed out that the opening of the crack will be counteracted by the reinforcement which crosses it.

This qualitative understanding of the crack behaviour under shear is not sufficient for an appropriate modelling which can be used in finite element programs. The lack of this accurate knowledge was the reason to start a new research project on the shear transfer in cracks in concrete.

This report will deal with information obtained from the literature, with the experimental investigation, with the physical model which has been derived, and with the analysis of experimental and theoretical results.

Finally, a model for the stress displacement behaviour of cracked concrete is derived on the basis of information published in the literature and of the authors' own results.

## 2 Information from the literature

An extensive survey of the accessible literature on the mechanisms of shear transfer in cracks in concrete was carried out and was published as a Stevin report [92] in 1978\*. The main conclusions of this survey were the following:

- Many basically different types of formulation to describe shear transfer in cracks are found. Several of these would lead to irrational results if applied to the analysis of shear critical structures.
- When the crack faces are subjected to a shear displacement a wedging action is developed, resulting in compressive stresses normal to the crack plane. Reinforcement crossing the crack or other restraint elements is activated, the forces in which must maintain equilibrium.
- Although the resistance to shear displacement of concrete interfaces, generally designated as aggregate interlock, has been investigated by a number of authors in various ways, hardly any attention has been given to the phenomenon of wedging action which provides the link between normal and shear stresses, on the one hand and crack opening and shear displacement on the other hand.
- With regard to the fundamental mechanism of shear transfer in cracks there are divergent opinions based on different test results. Laible, White and Gergely [43] distinguish between two levels of crack roughness: an overall roughness leading to overriding, and a local roughness producing an initially great resistance to shear displacement, but disappearing due to crushing under increasing stresses. Mattock [53] points out that the level of the sand particles is essential for the transfer of stresses in cracks, and he considers only overriding. Taylor [78] regards the ratio between aggregate strength and matrix strength as the most important variable which influences the roughness of the crack and, as such, the mechanical behaviour.
- The crack width is generally considered the most important variable influencing the shear stress-shear displacement relation. The concrete strength is believed also to be of major influence. Several opinions exist with regard to the influence of maximum particle size and aggregate type (rounded, crushed, lightweight).
- In cyclic loading a pronounced difference is observed between the first and subsequent cycles. In general, the first cycle exhibits an almost linear relation between shear stress and shear displacement, whereas the subsequent cycles show a strictly non-linear hardening type relation. The behaviour at small crack widths ( $< 0,25$  mm) is different from that at large crack widths. The most important parameters with regard to cyclic loading were found to be the concrete quality, the crack width, the number of cycles, and the maximum shear level. In spite of numerous experimental results a systematic investigation, especially for small crack widths, is not yet feasible.
- Dowel action is modelled by a beam on an elastic foundation. The critical variables are the free length of the dowel – depending upon the bond properties of the reinforcing bar, the inclination of the bar, and the concrete properties – and the foundation

\* References for all the literature consulted are given in Chapter 11 of this HERON issue.

- modulus of the concrete which decreases with increasing shear and normal displacements. Axial stress in the dowel bar reduces the resistance to shear displacement.
- Aggregate interlock and dowel action show similar relationships between shear stress and shear displacement. For small crack widths, aggregate interlock dominates over dowel action.
  - Although experimental results are amply available, they are still not sufficient for an accurate formulation of the basic relationships. Many data are incomplete or not accurate enough for this purpose, as the aims of most investigations were different from the aim of this research project.

In the period from 1978 up to now a few more publications have appeared ([98] to [102]) in this field. Most of them deal with cyclic shear and large crack widths in connection with seismic loading.

These results are well suited for practical application, but do not answer the question as to the fundamental understanding of the phenomenon.

As the general conclusion to be drawn from the literature survey it can be stated that no systematic investigation could be found which gives the relationships between shear stress, shear displacement, normal stress, and normal displacement (opening) of a crack in concrete starting at almost zero crack width and going up to about one millimeter. These relationships, as a function of the most important parameters, would provide the necessary information to be used in non-linear finite element computer programs for the analysis of concrete structures under service conditions and at limit states of stress or deformation.

### **3 Experimental investigation**

#### *3.1 General remarks*

Shear transfer in cracks in concrete is a rather complex phenomenon consisting of aggregate interlock and dowel action which are both influenced by the state of stress. While the shear force is applied to a specimen the force in the reinforcing bars which cross the crack develops according to the crack geometry and the restraint stiffness. Thus, the force in the reinforcement is not known in advance and should therefore be measured in order to determine the complete state of stress.

Unfortunately, it is not possible to measure the steel stress in an embedded reinforcing bar just at a crack when it is simultaneously pulled by normal forces and transversely pressed by dowel forces. Because of these experimental difficulties it was decided to carry out two different series of experiments: a first series on specimens with embedded bars and a second series with external restraint bars. In the first series, the force in the reinforcing bars has not been measured, but will be calculated on the assumption of the bond characteristic according to Rehm [95, 97]. In the second series, the force in the external restraint bars has been measured and will therefore immediately provide the normal forces on the crack plane. In the following, the two test series will be treated separately because of their entirely different nature.

## 3.2 Scope

### 3.2.1 Variables of tests with embedded bars

#### a. The reinforcement ratio

Several series of specimens were tested, in which the quantity of reinforcement across the crack was the only variable. To obtain systematic variation of the reinforcement ratio, all the series (which had a constant concrete quality) comprised at least 4 specimens reinforced with 2, 4, 6 and 8 stirrups  $\text{\O}8$  mm, which resulted in reinforcement ratios of 0.56%, 1.12%, 1.68% and 2.24%. In one series the range of reinforcement ratios was extended by adding a specimen with 2 stirrups  $\text{\O}4$  mm ( $\rho = 0.14\%$ ) and one with 3 stirrups  $\text{\O}16$  mm ( $\rho = 3.35\%$ ) to the series.

#### b. The bar diameter

In two of the series some additional tests were carried out with equal reinforcement ratios but different bar diameters: a specimens with 7 stirrups  $\text{\O}6$  mm ( $\rho = 1.10\%$ ) was compared with a specimen with 4 stirrups  $\text{\O}8$  mm ( $\rho = 1.12\%$ ), and in another case 2 stirrups  $\text{\O}16$  mm was compared with 8 stirrups  $\text{\O}8$  mm (both  $\rho = 2.23\%$ ). In this way it was observed whether an increase in bar diameter at a constant reinforcement ratio, which leads theoretically to less favourable bond behaviour (smaller restraint) and slightly reduced dowel action, would have an observable influence on the behaviour under loading.

#### c. The concrete strength

To compare the influence for the concrete strength, three mixes with the same maximum aggregate size of 16 mm were made, which were used for different standard series. The cube crushing strengths of the series were 20, 30/35 and 56  $\text{N/mm}^2$ . The mixes are given in Appendix 1.

#### d. The roughness of the crack plane

1. To check whether the accidental overall structure of the crack plane affects the behaviour of the specimen, a number of similar specimens were tested; if the inevitably always different crack structure were an important parameter, this would result in different behaviour under shear loading.
2. To test whether the shear transfer behaviour of a crack is primarily a function of the minor roughness of the faces of the crack rather than the major roughness or unevenness, as was stated in [53], a special gap-graded concrete mixture was designed. The aggregate grading curve of the mix was discontinuous: particles with sizes between 0.25 mm and 1.00 mm were excluded, while quartz powder was added to obtain a feasible mixture. The cube crushing strength was  $f_{cc} = 30 \text{ N/mm}^2$ , so that this series could be directly compared with one of the standard series with the same strength, but a continuous grading curve.
3. To study the effect of the roughness, due to the larger aggregate particles, a sanded lightweight concrete was used in one of the series, with a cube crushing

strength of  $34 \text{ N/mm}^2$ . In this series a lower roughness of the crack planes could be expected, since the cracks pass through the lightweight particles, but around the sand particles. The high-strength standard series ( $56 \text{ N/mm}^2$ ) could also be expected to have lower roughness, since in this concrete the bond strength between the cement paste and the aggregate particles is normally greater than the tensile strength of the aggregate. As a result the cracks were expected to intersect both the gravel and the sand particles, because of which the major and the minor roughness are less than in concretes with average strengths.

e. The effect of inclination of the stirrups to the crack plane

To study the effect of inclination of the reinforcement to the crack plane, a series was designed in which, for a constant cube crushing strength of  $34 \text{ N/mm}^2$ , 8 specimens all contained 2 stirrups  $\text{Ø} 8 \text{ mm}$ , but arranged at angles of  $45^\circ$ ,  $60^\circ$ ,  $67.5^\circ$ ,  $75^\circ$ ,  $105^\circ$ ,  $112.5^\circ$ ,  $120^\circ$  and  $135^\circ$  with the crack plane.

f. The presence of dowel action

To study the effect of elimination of dowel action, one series of four specimens (with 2, 4, 6 and 8 stirrups  $\text{Ø} 8 \text{ mm}$ ) was tested, in which the reinforcing bars were covered with soft sleeves over a distance of 20 mm on both sides of the crack. These sleeves consisted of layers of tape (width 40 mm) wrapped around the bars. The cube crushing strength was in the range of  $34\text{--}37 \text{ N/mm}^2$ , so that a direct comparison with the corresponding standard series was possible. Of course it has also to be taken into account that the restraint stiffness normal to the crack plane is reduced by the absence of bond over the wrapped part of the bar.

### 3.2.2 Variables of tests with external restraint bars

Series of specimens with the same concrete quality as in series with embedded bars were tested, so that results could be expected which could be directly used for the interpretation of the tests with embedded bars. Only the mix with a discontinuous grading curve was not repeated, since this gave results similar to those of normal concrete with the same strength. In the tests with embedded bars crack opening paths were observed only in a limited area. It appeared useful to gather values extending over a wider variation of crack opening paths and thus to obtain information on the shear and normal stress values for a great variety of shear and normal displacements. Therefore initial crack widths of 0.0, 0.2 and 0.4 mm were combined with varying values of the external restraint stiffness. The variation of this stiffness, however, could only be rather approximate, since it was not only a function of the stiffness of the restraint bars and plates, but also of the accidental stiffness of the sand-cement paste layer between anchorage plate and specimen.

### 3.3 Specimens

For both series push-off type specimens similar to those of Mattock [51] were used.

### 3.3.1 Specimens with embedded bars

In the first three series, specimens as shown in Fig. 1a were used; in the rest of the program, specimens as in 1b. The shear plane of all the specimens was  $36000 \text{ mm}^2$  ( $300 \text{ mm} \times 120 \text{ mm}$ ) in area. When loaded as indicated by the arrows, shear without moment is produced in the shear plane. The reinforcement crossing the shear plane was in the form of closed stirrups, lapped on one of the short sides. This was to ensure effective anchorage of the reinforcement on both sides of the shear plane. The specimens were cast in horizontal wooden moulds on their sides, so that at the time of casting the shear plane was vertical.

On the front and rear face metal strips for the attachment of measuring devices were cast in. Two days after casting, the specimens were demoulded and stored in an air-conditioned and temperature-controlled room with a constant relative humidity of 95% and a temperature of  $21^\circ \text{C}$ . One day before testing, the specimens were transported to the testing hall. The reinforcement provided to prevent failure in other parts of the specimens was arranged as shown in Fig. 2.

The reinforcing steel of the stirrups was a deformed Hi-Bond steel, the stress-strain diagrams of which are given in Appendix 2.

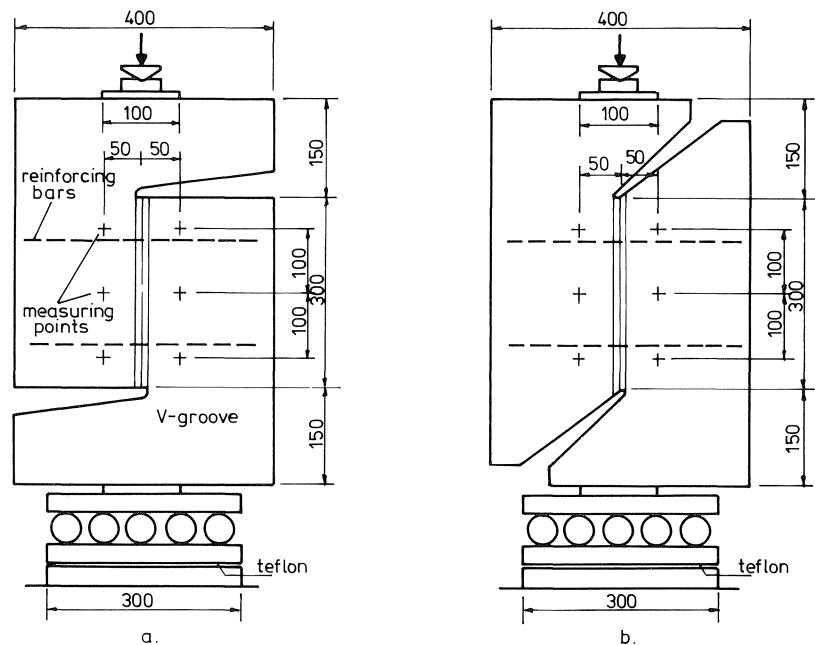


Fig. 1. Geometry of test specimens.

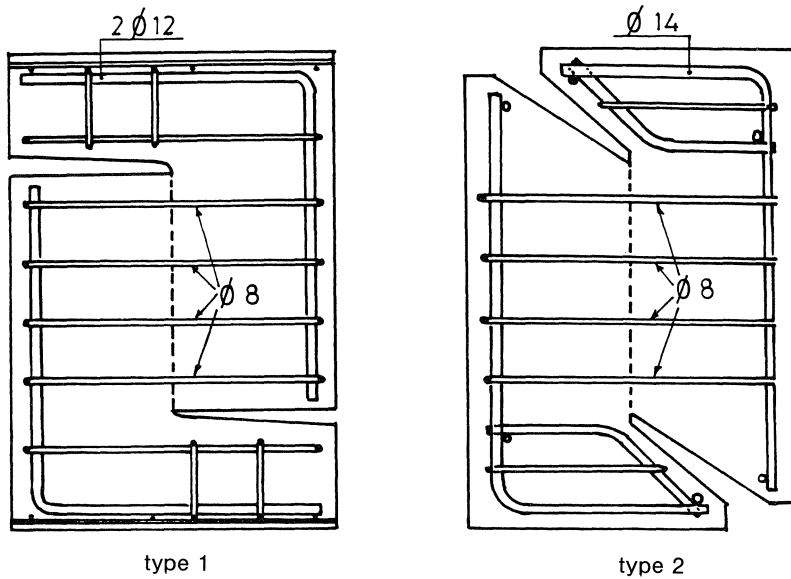


Fig. 2. Stirrups and additional reinforcement in both types of specimens.

### 3.3.2 Specimens with external restraint bars

For these tests, specimens with the same dimensions as in the series with embedded bars were used. On the small sides of the specimens steel plates were fixed by means of bolts, screwed in holes, formed at the time of casting by inserting plugs into the fresh concrete. The steel plates were stiffened by transverse ribs, welded to the free side of the plates. Between these plates four external restraint bars were fastened. A schematic view of such a specimen is given in Fig. 3.

Initially the stiffness of the restraining system was lower than expected, which was to be blamed on bad fitting of the restraint plates on the concrete surface of the short sides of the specimen. Therefore these sides were smeared with a rapidly hardening sand-

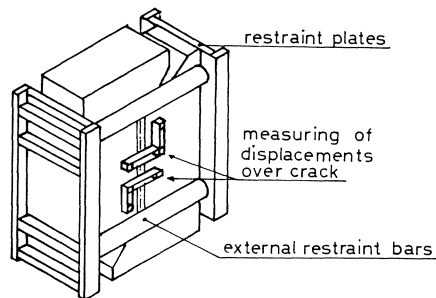


Fig. 3. Arrangement of restraint plates and bars on the specimens.

cement paste before fixing the plates. Although this technique resulted in higher stiffness values, values comparable with those attainable with the largest quantities of embedded reinforcement could not be obtained.

The arrangement was so designed that dowel action of the external bars was negligible. This was confirmed by measurements at the top and bottom of the bars just beside the restraint plate.

### 3.4 *Testing set-up and instrumentation*

Prior to the shear test, the specimens were cracked along the shear plane by splitting forces in the grooves on their front and rear faces. The crack width was measured during this operation by four electrical strain gauges so that the derived initial crack width could be achieved.

The actual tests were carried out in a hydraulic testing machine. As indicated in Fig. 4, the specimens were supported on roller bearings, whereas the load was applied to the specimen through knife hinges so that eccentricities could be avoided. The crack width and the shear displacements of the crack were measured on both sides with an accuracy of 0.01 mm. Fig. 4 gives a view of the loaded specimen and a close-up of the electrical strain gauges. Appendix 3 shows the whole loading equipment.

During the test, crack width and shear displacement were printed directly on a teleprinter. All the measurements were collected by a data acquisition system and processed by the Hewlett Packard XM21 laboratory computer.

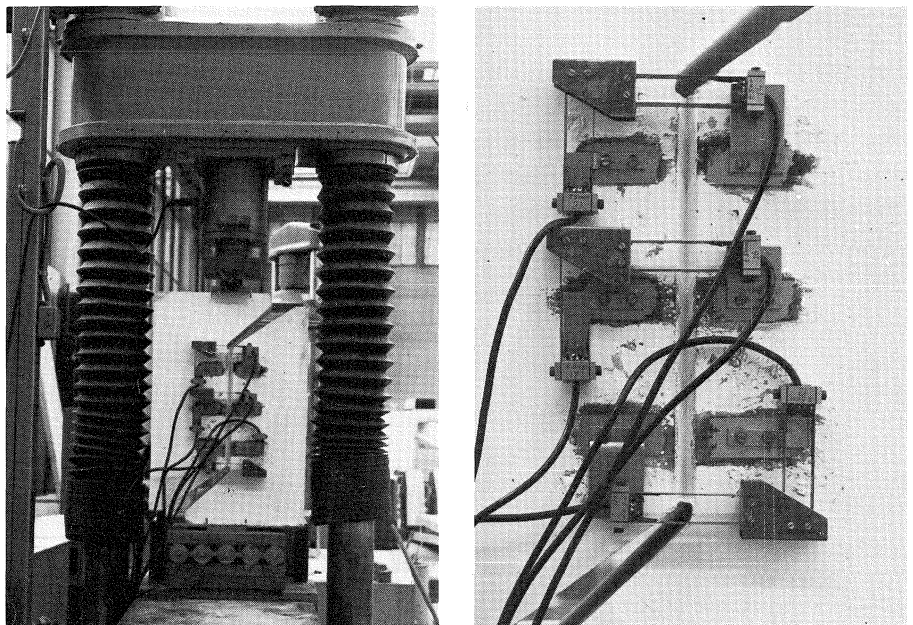


Fig. 4. A loaded specimen (left) and the electrical strain gauges (right).

### 3.5 Testing procedure

The pre-cracked specimens with an initial crack width of the order of 0.01 to 0.03 mm were subjected to a continuously increasing load. During the first three minutes the shear displacement rate was 0.004 mm/min, which was subsequently increased to 0.02 mm/min. The ultimate load was defined as the maximum load carried by the specimen during the test. After passing the top of the load-shear displacement curve the displacement rate was increased to 0.05 mm/min. The tests were ended when the shear displacement had reached a value of 2 mm. A few specimens were unloaded after passing the top of the curve, and subsequently reloaded in order to obtain some idea of the behaviour under repeated loading.

In some of the heavily reinforced specimens ( $\rho > 1.5\%$ ) spalling was observed at the ends of the shear plane. The total size of the spalling region (top + bottom) was always less than 60 mm.

Short cracks inclined to the main crack plane – as reported in [53] – were not observed in any of the specimens. Even for 3 stirrups  $\varnothing 16$  mm, corresponding to a reinforcement ratio of 3.35%, no inclined cracks developed.

### 3.6 Survey of experimental results

#### 3.6.1 Tests with embedded bars

For easier reading of the following results, the identifying code of the specimens will be explained. It consists of a six digit number, e.g., 130608. The first digit indicates the geometry of the specimen. 1 stands for a specimen of the type in Fig. 1a, 2 for the type in Fig. 1b, and 3 for the last type but with reinforcing bars covered with soft sleeves over a distance of 20 mm on both sides of the crack. The second digit indicates the type of mix used:

- 1 = Gravel concrete,  $D_{\max} = 16$  mm,  $f_{cc} = 30\text{--}35$  N/mm<sup>2</sup>
- 2 = Gravel concrete,  $D_{\max} = 16$  mm,  $f_{cc} = 29\text{--}30$  N/mm<sup>2</sup>, discontinuous grading
- 3 = Gravel concrete,  $D_{\max} = 16$  mm,  $f_{cc} = 56$  N/mm<sup>2</sup>
- 4 = Gravel concrete,  $D_{\max} = 16$  mm,  $f_{cc} = 20$  N/mm<sup>2</sup>
- 5 = Gravel concrete,  $D_{\max} = 32$  mm,  $f_{cc} = 38$  N/mm<sup>2</sup>
- 6 = Lightweight concrete, (Korlin A),  $f_{cc} = 24\text{--}38$  N/mm<sup>2</sup>

The third digit was a spare number, used during the tests themselves, but taken as 0 in this report.

The fourth digit indicates the number of stirrups crossing the crack plane. The fifth and sixth digit indicate the diameter of the stirrups in mm.

A full survey of all the tests with a detailed description of the variables and of the mechanical properties of the specimens is given in Appendix 4. These results will all be used in the analysis of chapters 4 and 8. Furthermore, all displacement measurements are documented in a Stevin report [93] and will also be used in the subsequent analyses.

### 3.6.2 Tests with external restraint bars

The identifying code of the specimens of this series refers to three characteristic data. The symbols representing three data, are separated by obliques (e.g., 3/.2/1.7). The first number indicates the type of mix which is given in Appendix 1. The second part of the code describes the initial crack width (0.2 in the example). The third part gives an indication of the restraint stiffness. Because this restraint stiffness is non-linear and its shape is particular to all individual tests, as an arbitrary indication the average restraining stress normal to the crack plane for a crack opening of 0.6 mm (including the initial crack width) is given. So in the example, for  $w = 0.6$  mm the restraining stress  $\sigma$  at the crack plane was 1.7 N/mm<sup>2</sup>.

A full survey of the series of tests on specimens with external restraint bars is given in Appendix 5; displacement measurements have been compiled in a Stevin report [93]. All these results will be used in the analyses in Chapters 5 and 6.

## 4 Results of tests with embedded bars

### 4.1 Tests with completely embedded bars

During the tests the applied shear force, the shear displacement, and the crack opening during the whole loading cycle were measured. From these measurements the shear stress-shear displacement relation ( $\tau$ - $\Delta$ -relation), and the crack opening path ( $\Delta$ - $w$ -relation) were deduced. On comparing the displacement measurements at different positions on the cracks, it could be concluded that the shear stress must have been approximately uniformly distributed over the whole shear area.

There are always two aspects which are interesting: the shear capacity of a crack under given circumstances and the crack displacements during the test, i.e., at certain shear stress levels depending upon the variables of the investigation. Both aspects will receive attention in the following short analysis of the results.

The influence of the amount of reinforcement for constant concrete quality on the shear stress-shear displacement relation and on the crack opening path is seen in Figs. 5 to 7. Two facts are evident from these diagrams: an increase of reinforcement leads to an increase of shear stress for the same shear displacement, and an increase of concrete quality acts in the same way. On the other hand, the crack opening path appears hardly to be influenced by the reinforcement ratio and by the concrete quality.

The maximum shear stresses which occurred in most of the tests at a shear displacement exceeding 0.5 mm are represented as a function of the concrete compressive strength  $f_{cc}$  and of the mechanical reinforcement ratio  $\rho f_{sy}$  in Fig. 8. Besides the results for gravel concrete with maximum particle size of 16 mm, the values for gravel concrete with 32 mm maximum aggregate size and for lightweight concrete are given. Only at low reinforcement ratios can a slight influence of these differences in concrete type be detected.

Another way to look at the results is to consider the crack opening at a certain rein-

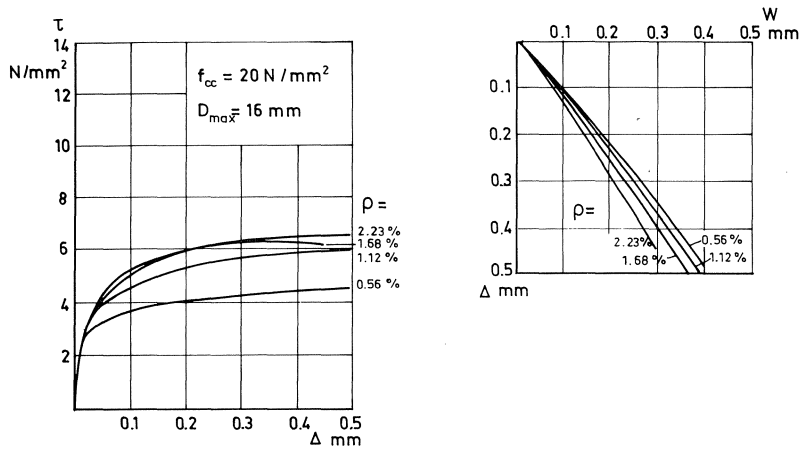


Fig. 5. Influence of the reinforcement ratio  $\rho$  on the shear stress-shear displacement relation (a) and on the crack opening path for mix No. 4 ( $f_{cc} = 20 \text{ N/mm}^2$ ).

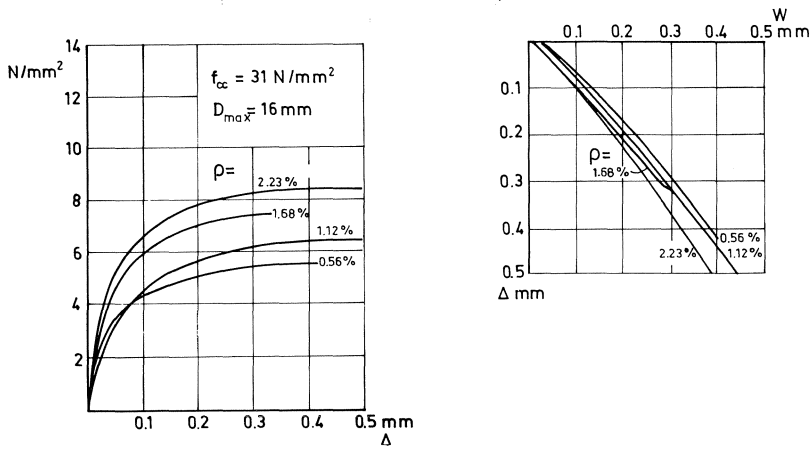


Fig. 6. The same as Fig. 5, but for mix No. 1 ( $f_{cc} = 30.7 \text{ N/mm}^2$ ).

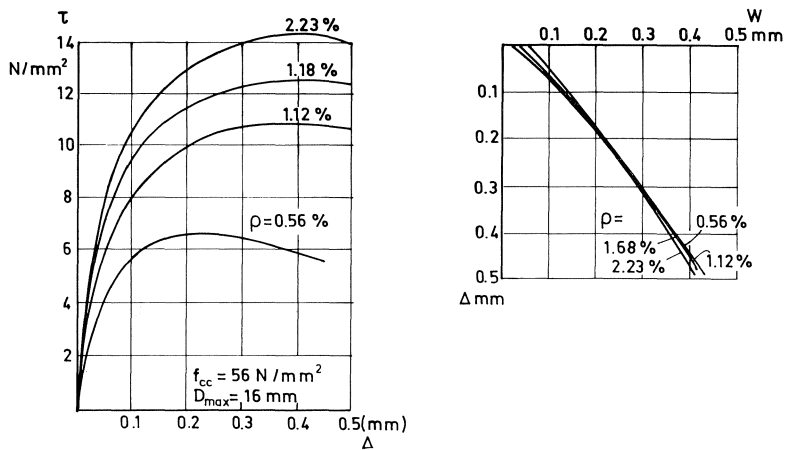


Fig. 7. The same as Fig. 5, but for mix No. 3 ( $f_{cc} = 56.1 \text{ N/mm}^2$ ).

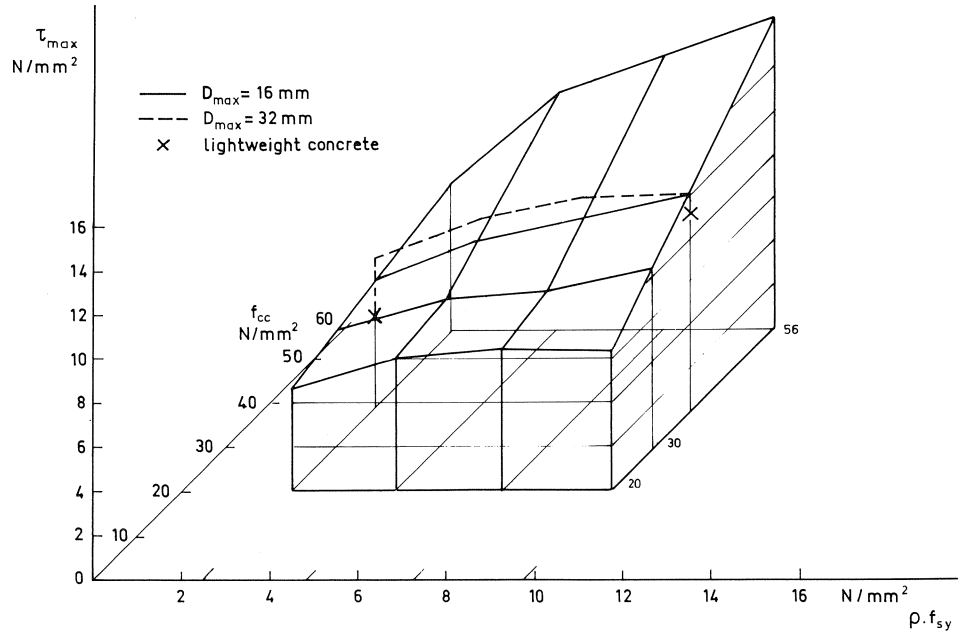


Fig. 8. Maximum shear stress as a function of concrete compressive strength  $f_{cc}$  and mechanical reinforcement ratio  $\rho \cdot f_{sy}$ .

forcement ratio under a certain shear stress, i.e., the dilatancy due to shear. For the mixes Nos. 2, 3, 4 and for the lightweight concrete those relations are plotted in Fig. 9.

It is seen that with increasing reinforcement the crack width decreases for all shear stresses. Lower concrete quality leads to larger cracks at the same shear stress. This phenomenon is due to the fact that in a low quality concrete only a few particles break through, resulting in a very rough crack surface and thus in a high degree of shear dilatancy. The smallest crack widths are obtained in lightweight concrete with a high reinforcement ratio ( $\rho = 2.23\%$ ), whereas with less reinforcement ( $\rho = 0.56\%$ ) the cracks are larger than in comparable gravel concrete also compared at the same shear force.

The diameter of the reinforcing bars was varied between 6 and 16 mm at constant reinforcement ratios. Within this range, the tests showed no significant influence of this parameter on the results. As far as the minor roughness of the crack plane is concerned, no significant difference between gap-graded concrete and continuously graded concrete could be discovered.

In order to complete the picture, the average displacement paths (average of the different reinforcement ratios) for all concretes are plotted in Fig. 10, where the range of crack width and shear displacement is extended to about 2 mm. There is a cluster of lines belonging to the mixes Nos. 4 and 2, to the gap-graded concrete and to the concrete with maximum aggregate size of 32 mm which show only small differences.

Contrary to these lines, mix No. 3 reveals slightly smaller crack widths, and light-

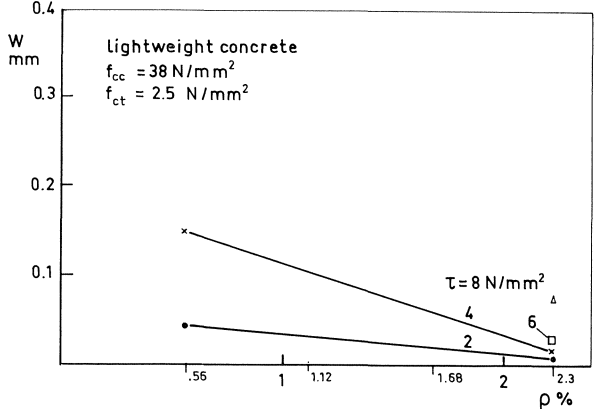
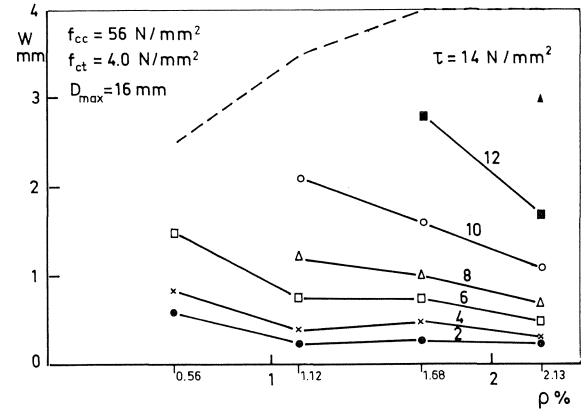
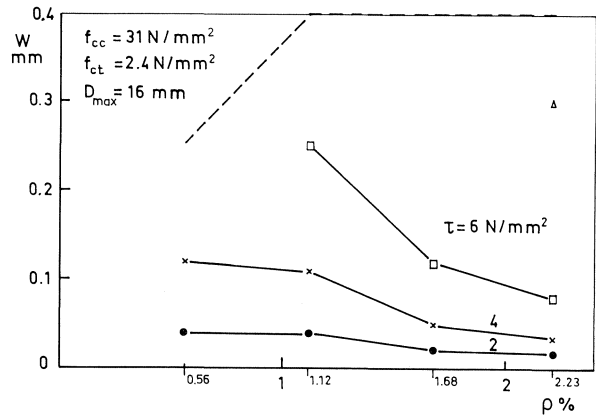
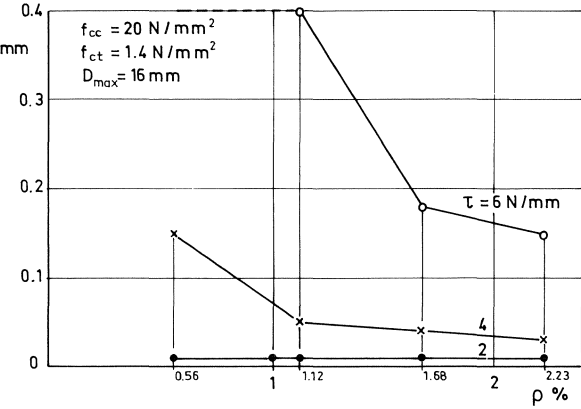


Fig. 9. Crack opening under a certain shear stress  $\tau$  as a function of the reinforcement ratio  $\rho$  for mix No. 1 to 3 and for lightweight concrete.

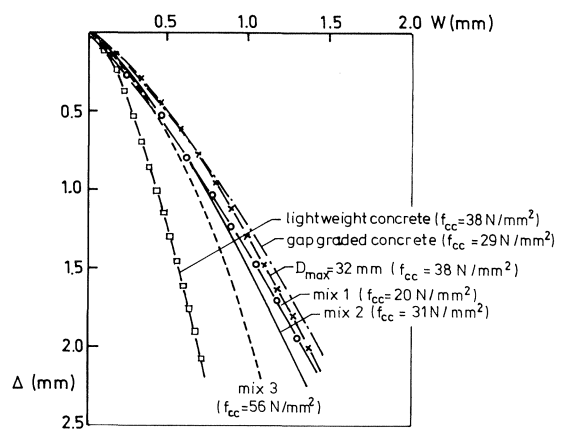


Fig. 10. Average crack opening paths for all mixes.

weight concrete shows the least crack widths at same shear displacements. It is apparent that the crack faces of the lightweight concrete and the high quality gravel concrete are less rough than those of the other mixes with low to medium quality and that therefore the shear dilatancy is less.

In a few tests the specimens were *unloaded and reloaded* immediately or after a couple of months. Fig. 11 and 12 show two examples of such tests, the first with immediate reloading and the second with a delay of five months.

In both diagrams it is obvious that the unloading path is not the same as the first loading path, i.e., a permanent set occurs because of friction and overriding of particles in the crack plane. As soon as the load during the second cycle has reached the original load level, the old path is followed which can clearly be seen in the shear to normal displacement diagrams.

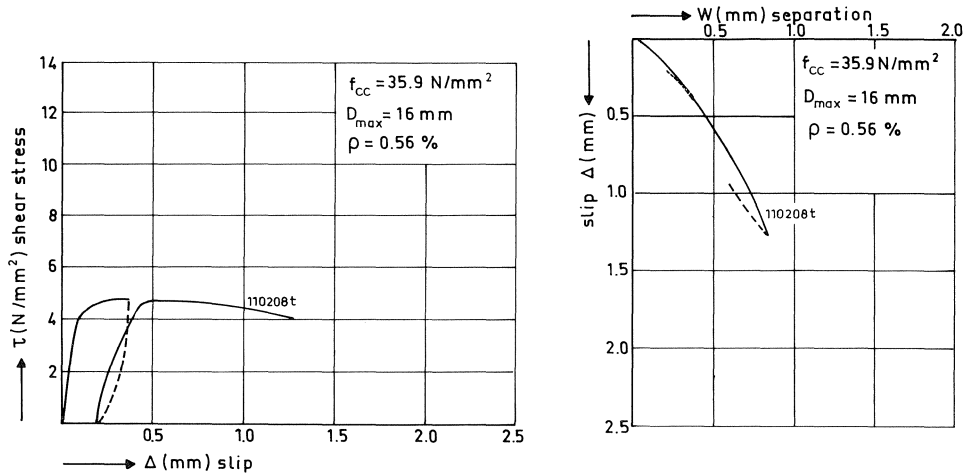


Fig. 11. Repeated loading immediately after unloading.

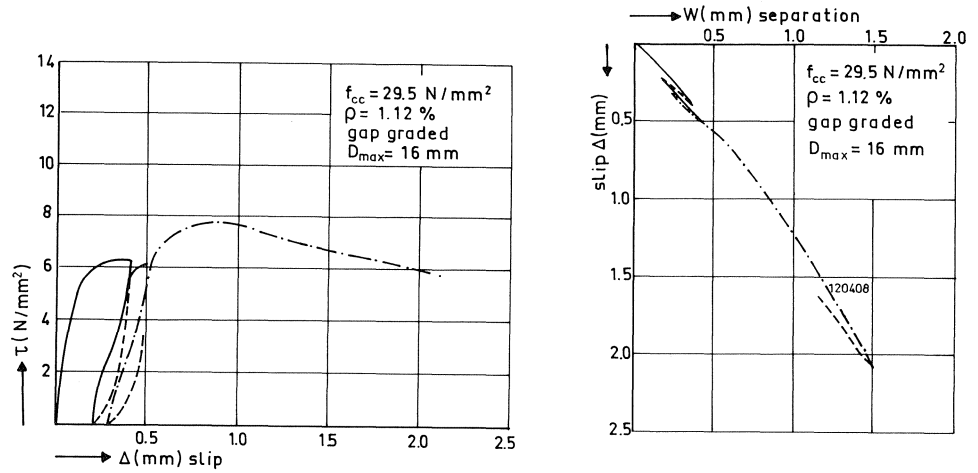


Fig. 12. Repeated loading with five months' delay.

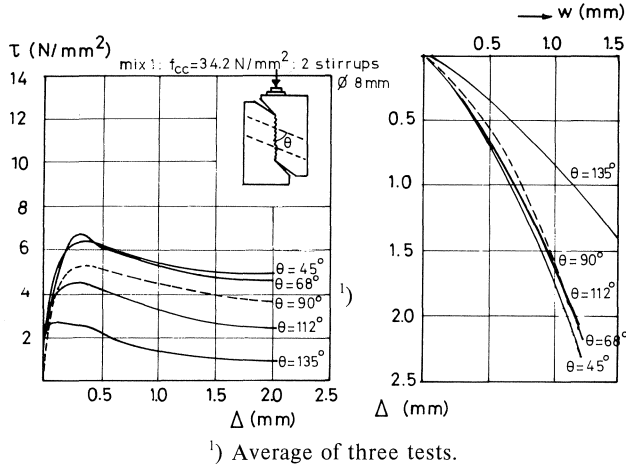


Fig. 13. Shear stress-shear displacement relation (left) and crack-opening path (right) at various angles of inclination  $\theta$ .

The continuous hardening during five months' after unloading increases the shear strength, as seen in Fig. 12. As far as the crack movement is concerned the influence of the strength increase is negligible.

The influence of the *bar inclination* in relation to the crack plane has been studied by varying the angle  $\theta$  from 45 to 135 degrees. Fig. 13 shows the effect on the shear stress-shear displacement relation and on the crack opening path. From these diagrams it emerges that the efficiency of the reinforcement increases with smaller angles of inclination, i.e. the shear capacity increases if the stirrups intersect the crack plane at angles smaller than 90 degrees. In the right hand diagram of Fig. 13 it is seen that the crack opening path only changed when the angle of inclination amounted 135 degrees. In all other cases it was not affected by the angle of inclination.

#### 4.2 Tests with bars with interrupted bond

In these tests, the reinforcing bars were provided with soft sleeves over a length of 40 mm, just 20 mm on both sides of the crack (Fig. 14) in order to prevent dowel action and deterioration of the concrete due to dowel action and pull-out forces of the reinforcing bars. Both effects are likely to affect the behaviour of the crack under shear forces. If these effects are eliminated, only aggregate interlock should provide shear resistance.

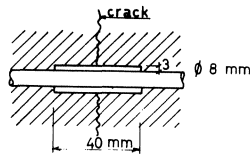


Fig. 14. Soft sleeves around the bars.

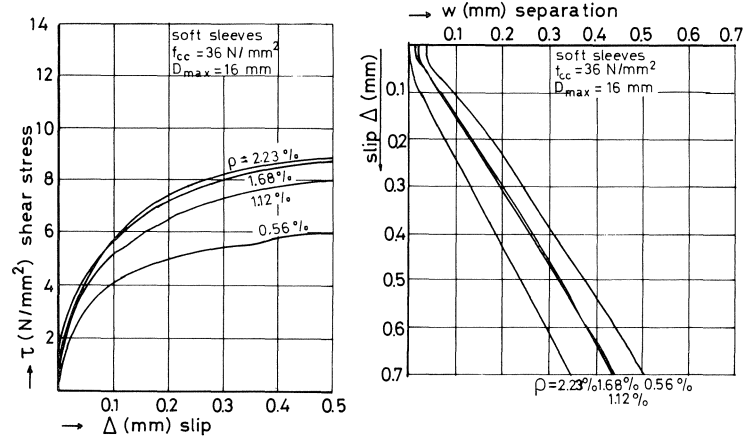


Fig. 15. Results of tests with bars with soft sleeves.

The test results at four reinforcement ratios for the same concrete quality are plotted in Fig. 15. From this figure it is clear that the amount of reinforcement, i.e. the lateral stiffness, influences the crack opening path: the more reinforcement the less does the crack opening become. Compared with Fig. 6, the absolute crack opening is also smaller in this case and the shear stresses at a given shear displacement is a little less than in the case with complete bond. The reason for this behaviour and the accompanying mechanism will be discussed in Chapter 7.

## 5 Results of tests with external restraint bars

As has been discussed before, the advantage of these tests is that the normal stresses acting on the crack plane can be measured directly on the restraint bars. Therefore, typical measurements in these tests are the shear stress, the normal stress, the crack opening and the shear displacement. A set of results for tests with concrete of mix No. 1 is given in Fig. 16 with a slip-crack width relation (a), a shear stress-shear displacement relation (b), and a normal stress-crack width relation (c). The seven specimens were made of the same concrete, but differed in initial crack width and restraint stiffness. The code of the lines  $\alpha/\beta/\gamma$  consists of  $\alpha$  which means the concrete mix,  $\beta$  the initial crack width in millimeters, and  $\gamma$  the normal stress in  $\text{N}/\text{mm}^2$  at an arbitrarily defined crack width of 0.6 mm. The influence of the initial crack width is evident: an increasing initial crack width leads to more shear displacement at the same shear stress and to a larger crack width at constant normal stress. Similar results are obtained with other concretes.

The most striking difference between these tests and the tests with embedded bars is that even a small difference in restraint stiffness results in a different crack opening path. It is believed that this has to be attributed to a locally reduced crack width around the reinforcing bars. This will be discussed later (Chapter 7.1).

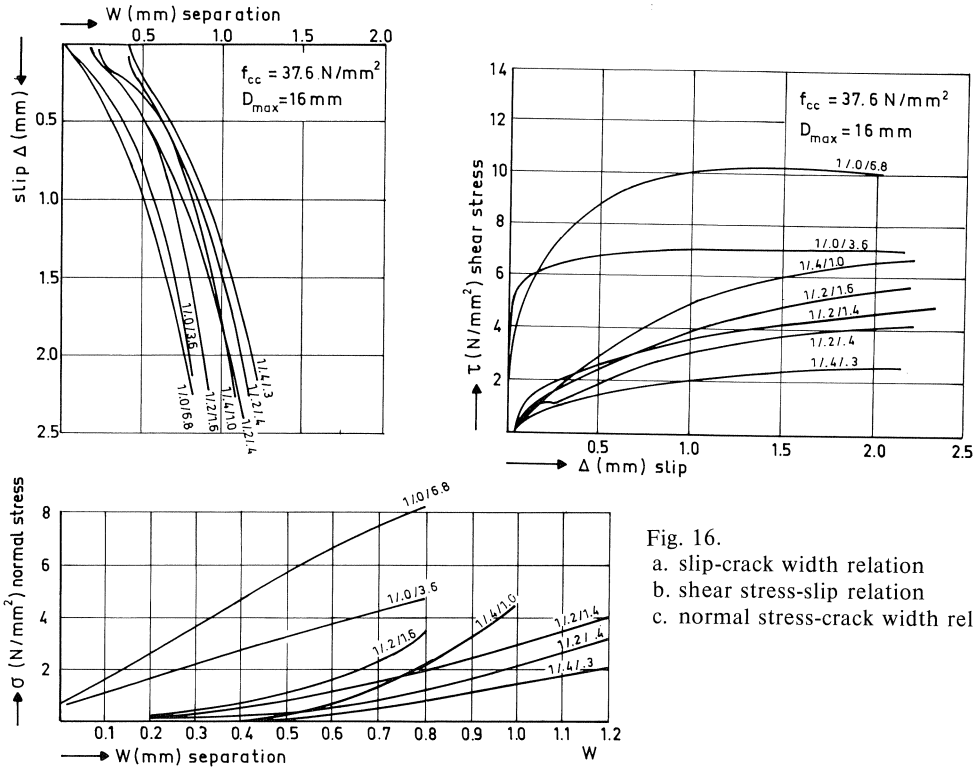


Fig. 16.  
a. slip-crack width relation  
b. shear stress-slip relation  
c. normal stress-crack width relation

Although all relations of Fig. 16 are non-linear, it is possible to deduce linear relations between the four variables shear stress, shear displacement, normal stress, crack opening, which fit the experimental data quite well.

The curves which fitted the results with the greatest accuracy are:

$$\tau = -\frac{f_{cc}}{30} + \{1.8w^{-0.80} + (0.234w^{-0.707} - 0.20) \cdot f_{cc}\} \Delta \quad (\tau > 0) \quad (1a)$$

and

$$\sigma = -\frac{f_{cc}}{20} + \{1.35w^{-0.63} + (0.191w^{-0.552} - 0.15) \cdot f_{cc}\} \Delta \quad (\sigma > 0) \quad (1b)$$

A comparison of these bilinear approximations with the experimental results of the various series are represented in Figs. 17 to 19 ( $\Delta$  and  $w$  in mm).

A regression analysis of the results of the experiments with lightweight concrete (mix 6) yielded the equations:

$$\tau = -\frac{f_{cc}}{80} + (1.495w^{-1.233} - 1) \cdot \Delta \quad (\tau > 0) \quad (2a)$$

and

$$\sigma = -\frac{f_{cc}}{40} + (1.928w^{-0.87} - 1) \cdot \Delta \quad (\sigma > 0) \quad (2b)$$

A comparison of these equations with the experimental results is given in Fig. 20 ( $\Delta$  and  $w$  in mm).

In the following diagrams these relations are plotted with the crack width  $w$  as a common parameter. To each line belong experimental results with a specific character, for instance:

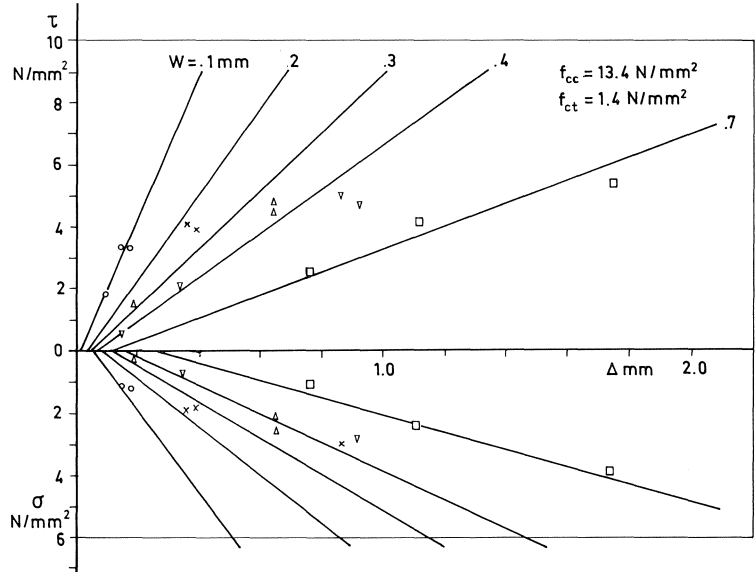


Fig. 17. Combination of shear stress  $\tau$ , normal stress  $\sigma$ , slip  $\Delta$ , and crack opening  $w$ , for concrete cube compressive strength of  $13.4 \text{ N/mm}^2$ .

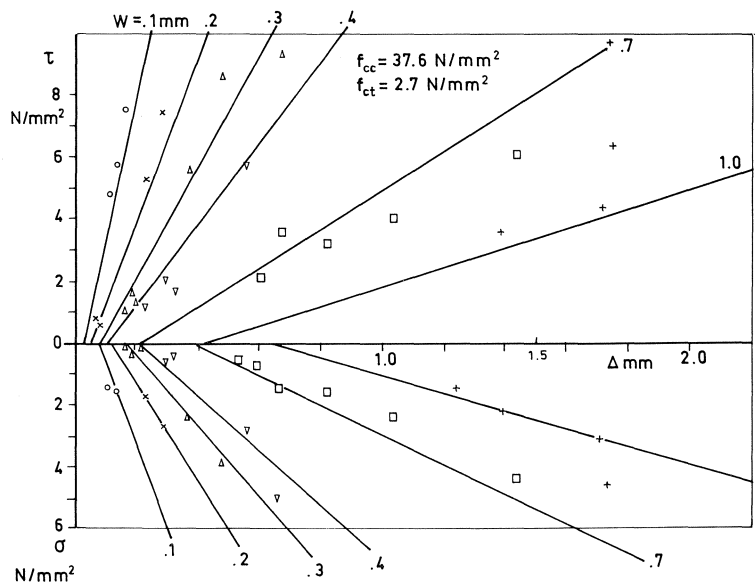


Fig. 18. The same as Fig. 17 for a compressive strength of  $37.6 \text{ N/mm}^2$ .

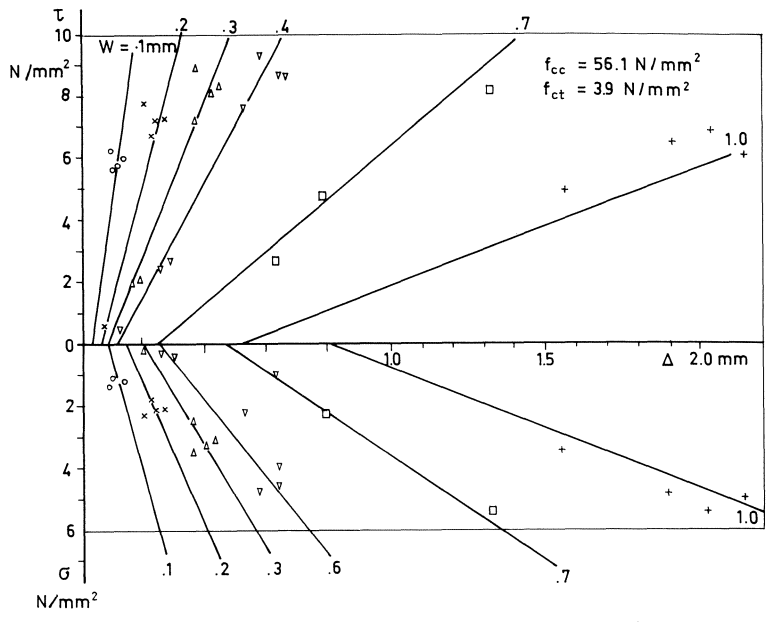


Fig. 19. The same as Fig. 17 for a compressive strength of 56.1 N/mm<sup>2</sup>.

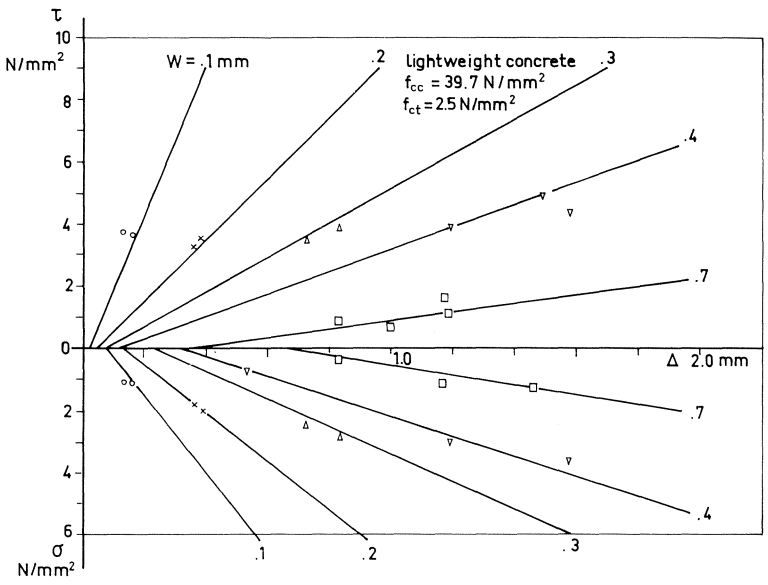


Fig. 20. The same as Fig. 17 for lightweight concrete with a compressive strength of 39.7 N/mm<sup>2</sup>.

the circle was measured at  $w = 0.1$  mm, the  $x$  at  $w = 0.2$  mm, the triangle with upper vertex at  $w = 0.3$  mm and so on.

These diagrams reveal some interesting features: suppose there is a normal stress of a certain value and there is a shear stress of a certain value, then a limit situation of equilibrium will occur when slip and crack width in both halves of the diagram are the same. If the shear stress were increased and the normal stress remained the same, failure would occur due to slip. On the other hand, if the normal stress were increased above the value belonging to a certain combination of  $\tau, \Delta, w$ , nothing would happen.

Another way to interpret the diagrams in regard to concrete type and quality is to take a certain slip  $\Delta$  and to look at the shear stress  $\tau$  and normal stress  $\sigma$  for a certain crack width  $w$ ; for instance,  $\Delta = 0.6$  mm and  $w = 0.3$  mm. Comparing the various gravel concretes, it can be seen that increasing concrete quality leads to higher shear and normal stresses. The lightweight concrete behaves differently, as can be observed by comparison of Fig. 20 with Fig. 18, relating to gravel concretes of approximately equal strength. Whereas for normal concrete the shear stress is  $9 \text{ N/mm}^2$  for this example and the accompanying normal stress is  $5 \text{ N/mm}^2$ , the corresponding stresses for lightweight concrete are  $2.5 \text{ N/mm}^2$  and  $1.8 \text{ N/mm}^2$  respectively. Generally speaking, lightweight concrete exhibits larger slip and less crack width in comparison with normal concrete at the same stress level.

This rather phenomenological interpretation of the test results will be followed by a fundamental treatise on aggregate interlock in the following chapters. There, the influence of the crack surface and the restraint stiffness will be discussed in detail.

## 6 Basic analysis of aggregate interlock

A fundamental model has been developed, based on a statistical analysis of the crack structure and the associated contact areas between the crack faces as a function of the displacements  $w$  and  $\Delta$ .

### 6.1 Fundamentals

Concrete can be represented as a two-phase system: in a matrix (hardened cement paste) a collection of aggregate particles are embedded. Generally the strength and stiffness of the aggregate particles are greater than those of the matrix. However, the contact area between the two materials, the bond zone, is the weakest link of the system. Hence, cracking occurs commonly through the matrix, but along the circumference of the aggregate particles. These particles are simplified to spheres, which can be intersected

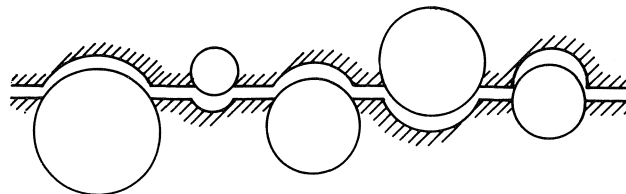


Fig. 21. Generally observed structure of a crack plane.

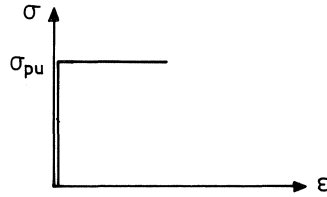


Fig. 22. Rigid-plastic stress-strain relation for the matrix material.

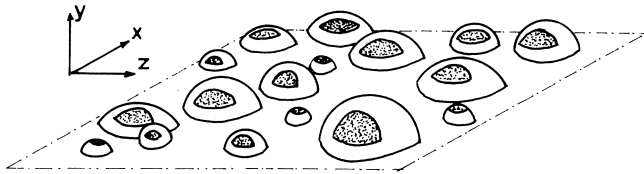


Fig. 23. Contact areas during shear displacement.

by the crack plane at all depths with the same probability. This results in a crack structure as represented in Fig. 21.

Considering this diagram and taking into account that the size of most particles is considerably greater than the crack width, it can be concluded that the “micro-roughness” of the crack, caused by the aggregate particles projecting from the crack plane, dominates the “macro-roughness” due to overall undulations of the crack faces. Therefore the overall crack plane is assumed to be a flat plane.

Hardened cement paste is a visco-elastic material: the deformations provoked by stresses are only partially elastic; for the other part they are plastic. Under multi-axial stresses, in the area between the aggregate particles in concrete, large plastic deformations can occur as a result of pore-volume reduction. Since the plastic deformations are expected to predominate over the elastic deformations, the stress-strain relation of the matrix material, consisting of hardened cement paste with aggregate particles smaller than 0.25 mm, is assumed to be rigid-plastic, as represented in Fig. 22.

The stress at which plastic deformation occurs is denoted by  $\sigma_{pu}$ . Hence it can be expected that, during shear displacement of the crack faces, contact areas develop on the surface of the particles, with interlocking between the crack faces, due to plastic deformation of the matrix. Fig. 23 shows the formation of this type of areas as a result of shear displacement in the direction of the X-axis. The stresses at these contact areas produce reactions in the directions of all the principal axes. On the assumption of spherical particles, the resulting component in the Z-direction is zero, just as for a real crack face, if the crack area is not too small. As a result it is possible to consider a cracked concrete body, as represented in Fig. 24a, as an assembly of a large number of slices each of finite width (Fig. 24c), and it is possible to deduce the overall behaviour of the crack by first studying the properties of this thin slice.

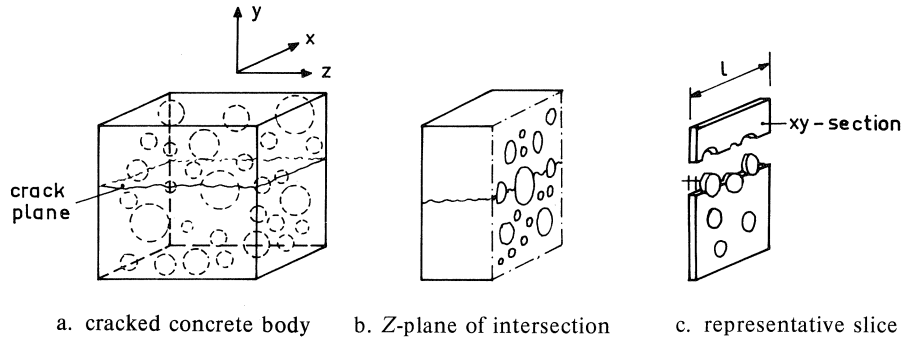


Fig. 24.

Fig. 25 shows a cross-section through a particle lying in a Z-plane in which there is a line of contact between the opposite crack faces. The projections of this line of contact on the X- and Y-directions are  $a_x$  and  $a_y$ . The shaded area represents that part of the matrix which has disappeared due to plastic deformation of the matrix. If the shear load on the plane of cracking is increased and crack opening is counteracted by restraining forces, a mechanism will develop which can be described as follows: The contact areas tend initially to slide; as a result of this sliding, the contact area is reduced, so that too high contact stresses occur. Hence, further plastic deformation occurs, until equilibrium of forces is obtained in the X- and Y-directions.

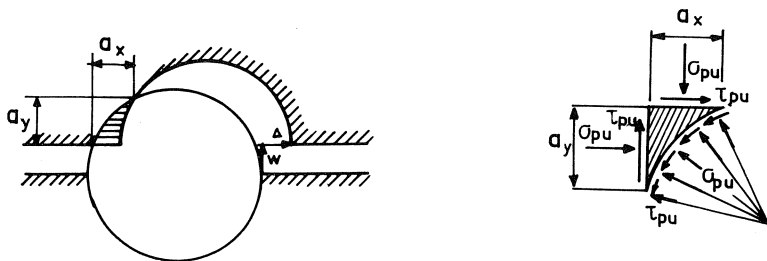
The stresses at the contact area are resolved into a stress  $\sigma_{pu}$ , normal to the contact area, and a stress  $\tau_{pu}$ , tangential to this area. The stresses  $\sigma_{pu}$  and  $\tau_{pu}$  are interrelated by the condition that the contact areas are about to slide. Therefore the equilibrium conditions are formulated, based on a uniform critical stress combination  $(\sigma_{pu}, \tau_{pu})$ , with

$$\tau_{pu} = \mu \cdot \sigma_{pu} \quad (3)$$

Next, the components of the contact forces in the X- and Y-directions can be derived, based on the previous assumptions.

Fig. 25b shows the equilibrium conditions at a particle surface. The reactions in X- and Y-direction can be formulated as

$$F_y = \sigma_{pu} \cdot a_x - \tau_{pu} \cdot a_y \quad (4a)$$



a. contact area between matrix and aggregate

b. stress conditions

Fig. 25.

$$F_x = \sigma_{pu} \cdot a_y + \tau_{pu} \cdot a_x \quad (4b)$$

Inserting  $\tau_{pu}$  from (3) into these equations and subsequently summing all particle contributions, the total resistance of the crack area considered (with a unit width  $dz = 1$  according to Fig. 24c) can be formulated as

$$\Sigma F_y = \sigma_{pu} (\Sigma a_x - \mu \Sigma a_y) \quad (5a)$$

$$\Sigma F_x = \sigma_{pu} (\Sigma a_y + \mu \Sigma a_x) \quad (5b)$$

The values  $\sigma_{pu}$  and  $\mu$  are material constants, whilst the values  $\Sigma a_x$  and  $\Sigma a_y$  have to be calculated. The way to do this will now be shown.

The aggregate in the concrete used in the experiments was distributed according to the Fuller grading curve. This cumulative distribution function is represented by

$$P = \sqrt{\frac{D}{D_{\max}}} \quad (6)$$

in which  $p$  denotes the fraction passing a sieve with an aperture diameter  $D$ , while  $D_{\max}$  is the diameter of the largest aggregate particle. The probability that an arbitrary point in the concrete is located in an aggregate particle is denoted by  $P = p_k$ . Properly  $p_k$  is the ratio between the total volume of the aggregate and the concrete volume.

On the basis of (6) it is possible to derive also another function, namely, the probability that an arbitrary point in the  $Z$ -plane (Fig. 24c) is located within an intersection circle with a diameter  $D < D_0$ . This function is:

$$P_c(D < D_0) = p_k (1.065 D_0^{0.5} D_{\max}^{-0.5} - 0.053 D_0^4 D_{\max}^{-4} - 0.012 D_0^6 D_{\max}^{-6} - 0.0045 D_0^8 D_{\max}^{-8} - 0.0025 D_0^{10} D_{\max}^{-10}) \quad (7)$$

This is graphically represented in Fig. 26. (All mathematical derivations for the functions in this chapter are given in [94]).

The average length of the intersection line AB for a circle with a diameter  $D_0$ , crossed by the crack, is (Fig. 27):

$$\bar{s} = \frac{\pi D_0}{4} \quad (8)$$

Considering a crack section (intersection of the crack plane and the  $Z$ -plane, Fig. 24c) of unit length, the probability density function for the expected part of that length contain-

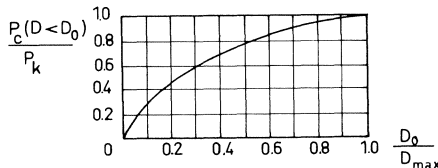


Fig. 26. Cumulative distribution function for the diameter of the intersected circles in a  $z$ -plane (Fig. 24c).

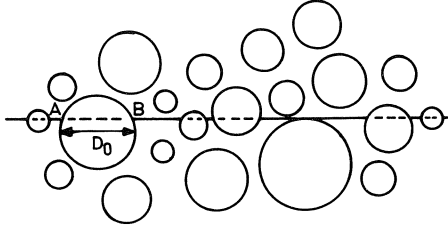


Fig. 27. Circles of intersection crossed by the crack.

ing only points which are located in an intersection circle with a diameter  $D_0$  can be obtained by multiplying this unit length by  $P'_c(D_0)$  where  $P'_c(D_0) = \partial P_c(D < D_0) / \partial D_0$  (eq. 7); hence:

$$l(D_0) = P'_c(D_0) \cdot 1 = P'_c(D_0)$$

Consequently the probability density function for the expected number of intersection circles with a diameter  $D_0$  in the  $Z$ -plane, which intersect also the unit crack length, can be obtained from (8) and (9) as

$$n(D_0) = \frac{P'_c(D_0)}{0.25\pi D_0} \quad (10)$$

Subsequently, the contact area for such an intersection circle with a diameter  $D_0$  is derived as a function of the crack width  $w$  and the shear displacement  $\Delta$ . There are three possibilities (Fig. 28).

The following expressions are found for the values  $\Delta_0$  and  $\Delta_b$ :

$$\begin{aligned} \Delta_0 &= \sqrt{R^2 - u^2} - \sqrt{R^2 - (u + w)^2} \\ \Delta_b &= \sqrt{2Rw - w^2} \end{aligned} \quad (11)$$

The projected contact areas  $a_x$  and  $a_y$  are:

for  $0 < \Delta < \Delta_0$ :

$$a_x = a_y = 0$$

for  $\Delta_0 < \Delta < \Delta_b$ :

$$\begin{aligned} a_y &= \sqrt{R^2 - \frac{1}{4}(w^2 + \Delta^2)} \frac{\Delta}{\sqrt{w^2 + \Delta^2}} - \frac{1}{2}w - u \\ a_x &= \frac{1}{2}\Delta - \sqrt{R^2 - \frac{1}{4}(w^2 + \Delta^2)} \frac{w}{\sqrt{w^2 + \Delta^2}} + \sqrt{R^2 - (u + w)^2} \end{aligned} \quad (12)$$

for  $\Delta > \Delta_b$ :

$$\begin{aligned} a_y &= R - (u + w) \\ a_x &= \sqrt{R^2 - (u + w)^2} \end{aligned}$$

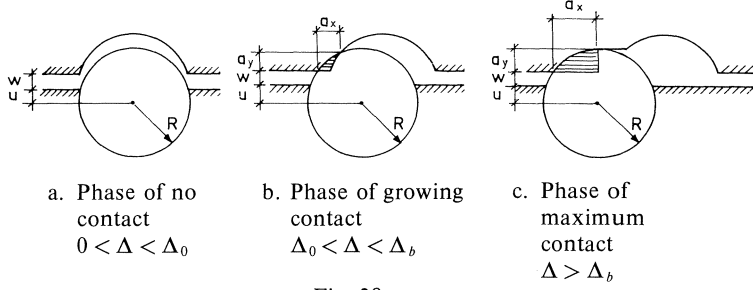


Fig. 28.

The equations (12) contain the embedment depth  $u$  as a variable. Assuming that all values of  $u$  can occur with the same probability, it is also possible to calculate the most probable average contact areas  $\bar{a}_x$  and  $\bar{a}_y$  (functions of  $D$ ,  $w$  and  $\Delta$ ).

So, if the crack faces are shifted with regard to each other ( $w$ ,  $\Delta$ ), for any intersection circle ( $D$ ) the most probable values of  $\bar{a}_{xD}$  and  $\bar{a}_{yD}$  are known. If  $D_{\min}$  is the smallest intersection circle which provides contact under the given conditions ( $w$ ,  $\Delta$ ), and  $D_{\max}$  is the largest intersection circle which occurs in the concrete mixture, the total contact area for a unit length and a unit width of the crack plane can then be calculated as

$$A_x = \Sigma a_x = \int_{D_{\min}}^{D_{\max}} n(D) \bar{a}_{xD} dD$$

$$A_y = \Sigma a_y = \int_{D_{\min}}^{D_{\max}} n(D) \bar{a}_{yD} dD \quad (13)$$

in which  $n(D)$  is taken from (10).

Evaluation of these equations (see [94]) gives:

Case A:  $\Delta < w$

$$A_y = \int_{\frac{w^2 + \Delta^2}{\Delta}}^{D_{\max}} p_k \cdot \frac{4}{\pi} \cdot F\left(\frac{D}{D_{\max}}\right) \cdot G_1(\Delta, w, D) \cdot dD \quad (14)$$

$$A_x = \int_{\frac{w^2 + \Delta^2}{\Delta}}^{D_{\max}} p_k \cdot \frac{4}{\pi} \cdot F\left(\frac{D}{D_{\max}}\right) \cdot G_2(\Delta, w, D) \cdot dD \quad (15)$$

Case B:  $\Delta > w$

$$A_y = \int_{\frac{w^2 + \Delta^2}{2w}}^{\frac{w^2 + \Delta^2}{w}} p_k \cdot \frac{4}{\pi} \cdot F\left(\frac{D}{D_{\max}}\right) \cdot G_3(\Delta, w, D) \cdot dD$$

$$+ \int_{\frac{w^2 + \Delta^2}{w}}^{D_{\max}} p_k \cdot \frac{4}{\pi} \cdot F\left(\frac{D}{D_{\max}}\right) \cdot G_1(\Delta, w, D) \cdot dD \quad (16)$$

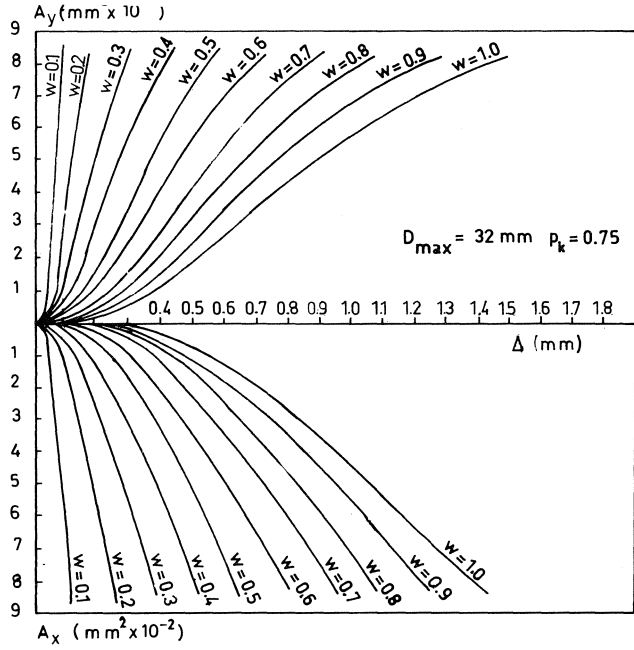


Fig. 29. Total projected contact areas  $A_y$  and  $A_x$  for  $1 \text{ mm}^2$  crack plane, as a function of crack width  $w$  and shear displacement  $\Delta$ , calculated with the equations (14–17).

$$\begin{aligned}
 A_x = & \int_{2w}^{\frac{w^2 + \Delta^2}{w}} p_k \cdot \frac{4}{\pi} \cdot F \left( \frac{D}{D_{\max}} \right) \cdot G_4(\Delta, w, D) \cdot dD \\
 & + \int_{\frac{w^2 + \Delta^2}{w}}^{D_{\max}} p_k \cdot \frac{4}{\pi} \cdot F \left( \frac{D}{D_{\max}} \right) \cdot G_1(\Delta, w, D) \cdot dD
 \end{aligned} \quad (17)$$

with

$$\begin{aligned}
 G_1(\Delta, w, D) &= D^{-3} \left( \sqrt{D^2 - (w^2 + \Delta^2)} \frac{\Delta}{\sqrt{w^2 + \Delta^2}} \cdot u_{\max} - w \cdot u_{\max} - u_{\max}^2 \right) \\
 G_2(\Delta, w, D) &= D^{-3} \left\{ (\Delta - \sqrt{D^2 - (w^2 + \Delta^2)}) \frac{w}{\sqrt{w^2 + \Delta^2}} \cdot u_{\max} + (u_{\max} + w) \right. \\
 & \quad \left. \sqrt{\frac{1}{4}D^2 - (w + u_{\max})^2} - w \sqrt{\frac{1}{4}D^2 - w^2} + \frac{1}{4}D^2 \arcsin \frac{w + u_{\max}}{\frac{1}{2}D} \right. \\
 & \quad \left. - \frac{D^2}{4} \arcsin \frac{2w}{D} \right\} dD \\
 G_3(\Delta, w, D) &= D^{-3} \left( \frac{1}{2}D - w \right)^2 \\
 G_4(\Delta, w, D) &= D^{-3} \left( \frac{\pi}{8} D^2 - w \sqrt{\frac{1}{4}D^2 - w^2} - \frac{D^2}{4} \arcsin \frac{2w}{D} \right)
 \end{aligned}$$

$$\begin{aligned}
F \left( \frac{D}{D_{\max}} \right) &= 0.532 \left( \frac{D}{D_{\max}} \right)^{0.5} - 0.212 \left( \frac{D}{D_{\max}} \right)^4 - 0.072 \left( \frac{D}{D_{\max}} \right)^6 \\
&\quad - 0.036 \left( \frac{D}{D_{\max}} \right)^8 - 0.025 \left( \frac{D}{D_{\max}} \right)^{10} \\
u_{\max} &= \frac{-\frac{1}{2}w(w^2 + \Delta^2) + \frac{1}{2}\sqrt{w^2(w^2 + \Delta^2)^2 - (w^2 + \Delta^2)\{(w^2 + \Delta^2)^2 - \Delta^2 D^2\}}}{(w^2 + \Delta^2)}
\end{aligned}$$

Integration of (14-17) was performed numerically. Fig. 29 shows the result of a calculation for a concrete with a maximum aggregate particle of 32 mm and  $p_k$  value equal to 0.75.

## 6.2 Comparison between theory and experiments

The relations between the stresses in a crack, on the one hand, and the displacement components, on the other hand, have earlier been formulated as (see also eq. (5))

$$\begin{aligned}
\sigma &= \sigma_{pu}(A_x - \mu \cdot A_y) \\
\tau &= \sigma_{pu}(A_y + \mu \cdot A_x)
\end{aligned} \tag{18}$$

in which  $A_x$  and  $A_y$  depend on the crack width  $w$ , the shear displacement  $\Delta$ , the maximum particle diameter  $D_{\max}$  and the total aggregate volume per unit volume of the concrete  $p_k$ , as expressed in the functions (14-17). The parameters  $\sigma_{pu}$ , the matrix yielding strength, and  $\mu$ , the coefficient of friction, are established by fitting the equations (18) to the experimental results. It appeared that the best results are obtained for a friction coefficient of  $\mu = 0.4$  for all mixes. This value is of the same order as was experimentally established by Weiss [96] in friction tests on concrete, mortar, and particle surfaces. The matrix yielding stress  $\sigma_{pu}$ , which has to be inserted to get optimal fitting, depends on the uniaxial concrete strength. The best results are obtained for

$$\sigma_{pu} = 6.39f_{cc}^{0.56} \text{ (N/mm}^2\text{)} \tag{19}$$

The matrix yielding strength turns out to be somewhat higher than the strength of the concrete itself. This must be regarded as regular: the weakest link of a hardened concrete is the interface between the aggregate particles and the matrix, where microcracks initiate the deterioration of the concrete; as a result, the concrete strength is lower than the strength of its constituting components. Also the fact that the ratio between matrix strength and concrete strength decreases with increasing concrete strength, as results from (19), is a generally observed phenomenon. All the experimental results were found to be well described by the equations (14-17) with the material constants  $\mu = 0.4$  and  $\sigma_{pu}$  from (19). Examples are given for two mixtures (Figs. 30 and 31). It must be emphasized that, to fit the equations (18) to the experimental results, only two degrees of freedom exist ( $\mu, \sigma_{pu}$ ), so that only two lines per diagram (e.g., for  $w = 1.0$  mm) can actually be fitted. The fact that all other lines are found automatically to fit the experimental results very well supports the validity of the theory.

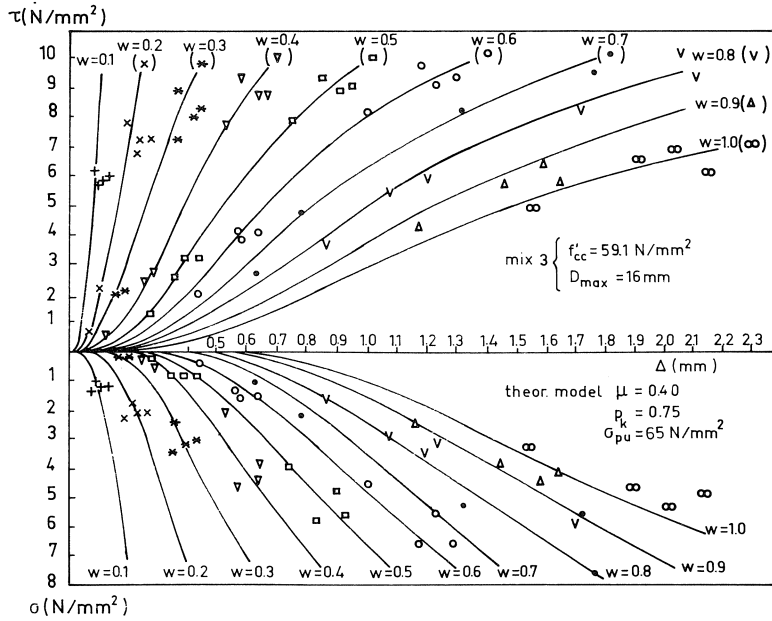


Fig. 30. Comparison between experimental values for a concrete with  $f'_{cc} = 59 \text{ N/mm}^2$ ,  $D_{max} = 16 \text{ mm}$  and theoretical values, with  $p_k = 0.75$ ,  $\mu = 0.40$  and  $\sigma_{pu} = 65 \text{ N/mm}^2$ .

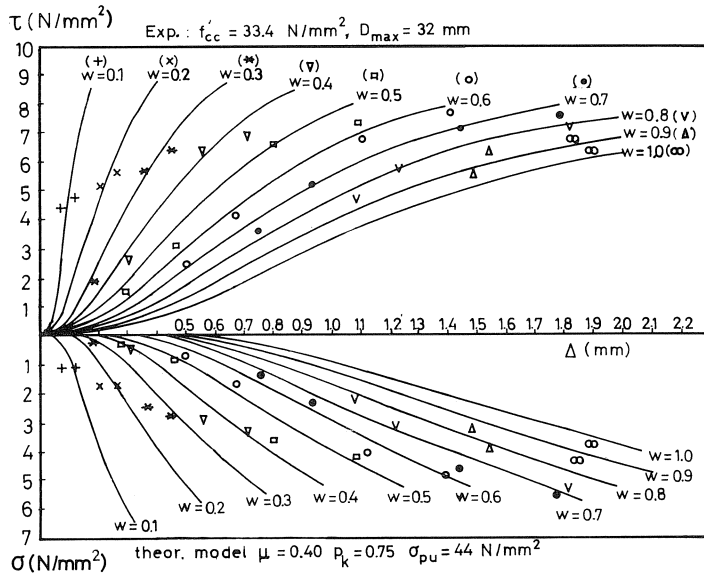


Fig. 31. Comparison between experimental values for a concrete with  $f'_{cc} = 33 \text{ N/mm}^2$ ,  $D_{max} = 32 \text{ mm}$  and theoretical values, with  $p_k = 0.75$ ,  $\mu = 0.40$  and  $\sigma_{pu} = 44 \text{ N/mm}^2$  (experimental values corrected with regard to elastic deformation of the concrete between crack and measuring points (Fig. 1): this was not yet done in [94]).

### 6.3 Further analysis of aggregate interlock

The model which has been developed is in adequate agreement with the experimental results. As such it can be used for parameter studies, yielding a better insight into the fundamental mechanics of aggregate interlock.

a. The role of the friction between aggregate and matrix:

It was shown that equilibrium in the contact area was obtained by combinations of normal (yielding) stresses and shear (friction-) stresses. It was shown that a friction coefficient equal to 0.4 resulted in the best fitting of the curves to the experimental results. By doing a calculation with a friction coefficient  $\mu = 0$  the influence of friction can be visualized. A calculation was carried out for a mix with maximum aggregate size  $D_{max} = 16$  mm,  $\sigma_{pu} = 50$  N/mm<sup>2</sup> corresponding with  $f_{cc} = 40$  N/mm<sup>2</sup>,  $p_k = 0.75$  and  $\mu = 0.0$  resp. 0.4. The results of this calculation are shown in Fig. 32 for some crack widths ( $w = 0.2, 0.6$  and  $1.0$  mm).

It is seen that the friction increases the shear stress by up to about 50%, whereas the normal restraint stresses to provide equilibrium are reduced.

b. The contribution of the various aggregate fractions to the transfer of stresses in a crack:

By a slight modification in the derivation of the equations representing the relations between stresses and displacements in the crack, it is possible to ascertain the contribution of only a part of the aggregate particles.

An example is given in Fig. 33. The contributions of a number of fractions have been established and represented for a small (0.1 mm), an average (0.6 mm) and a large (1

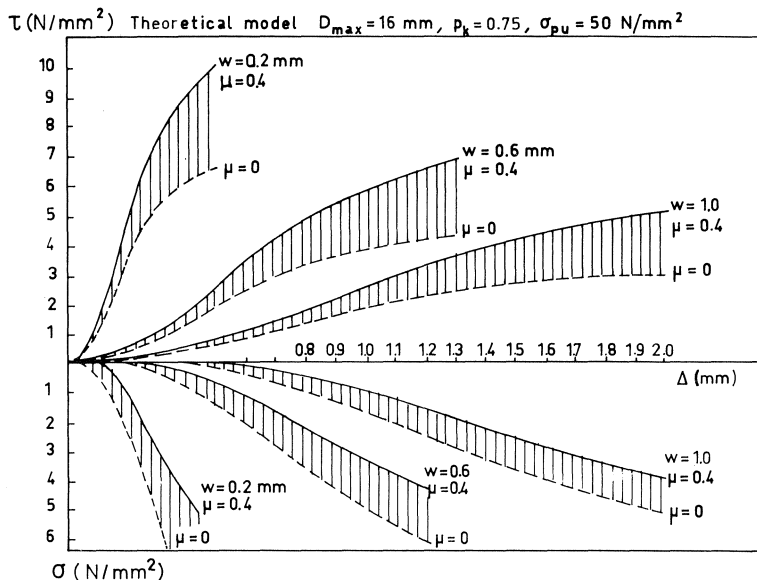


Fig. 32. The role of friction between aggregate and matrix in the transfer of stresses in a crack, for a concrete with  $D_{max} = 16$  mm and  $f_{cc} = 40$  N/mm<sup>2</sup>.

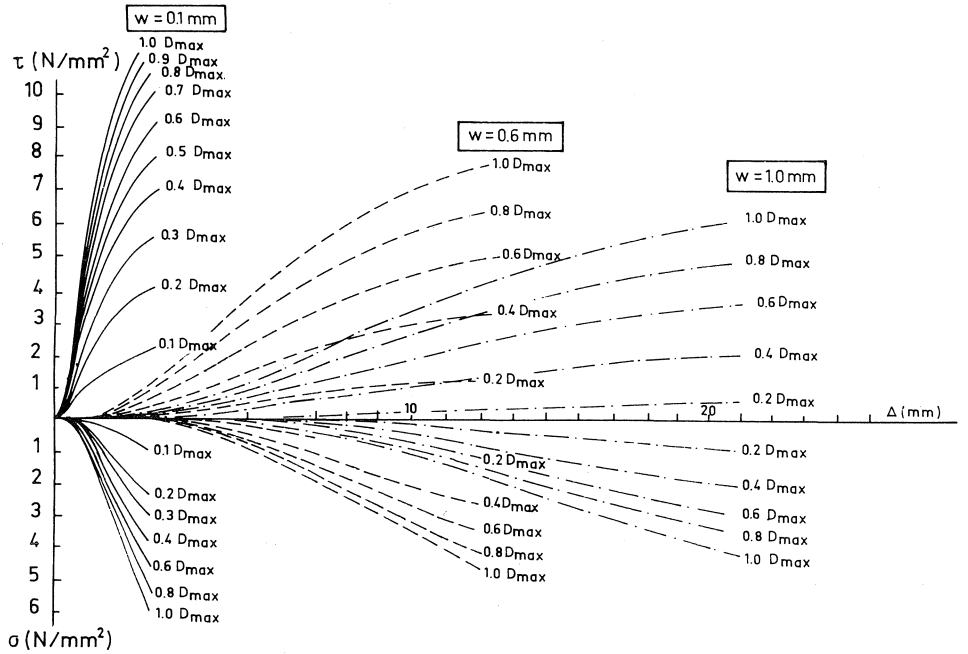


Fig. 33. Contribution of the various aggregate fractions to the transfer of stresses in cracks for crack widths  $w = 0.1$  mm,  $0.6$  mm and  $1.0$  mm for a concrete with  $f_{cc} = 32$  N/mm<sup>2</sup> and  $D_{max} = 32$  mm.

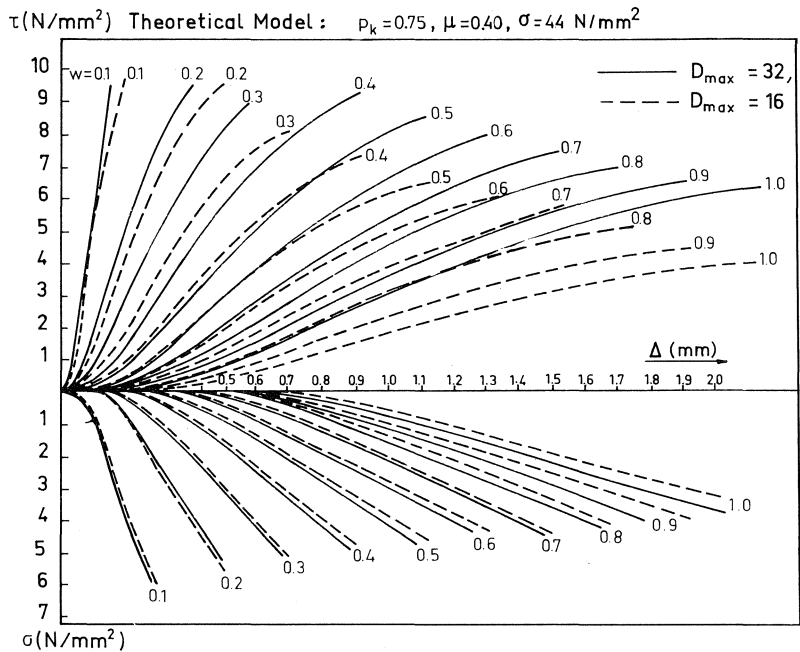


Fig. 34. The effect of the maximum aggregate particle size on the transfer of stresses in a crack. Concrete strength  $f_{cc} = 32$  N/mm<sup>2</sup>, maximum diameter  $D_{max} = 16$  and  $32$  mm.

mm) crack width, for a mix with a cube crushing strength of  $f_{cc} = 32 \text{ N/mm}^2$  and a maximum particle diameter of  $D_{max} = 32 \text{ mm}$  (inserted values  $\sigma_{pu} = 44 \text{ N/mm}^2$ ,  $\mu = 0.40$ ,  $p_k = 0.75$ ).

The curves in these diagrams represent the relations between  $\sigma$ ,  $\tau$ ,  $w$  and  $\Delta$  if only the particles with a diameter between 0 and a varying fraction of  $D_{max}$  are considered. It is seen that the small aggregate fractions lose importance as the crack width increases.

c. Scale effect of the aggregate:

To obtain some idea of the effect of the scale of the aggregate, two mixtures were compared. Both had the same properties, except for the maximum particle diameter, which was 16 mm and 32 mm respectively. The results of this comparison are shown in Fig. 34. It is seen that the normal stress  $\sigma$  is not very susceptible to this variation, but that the shear stress  $\tau$  is more affected according as the crack width is greater. This tendency is confirmed by the results of the experimental part of this investigation.

d. Influence of grading curve:

In the previous analyses and in the experiments a Fuller curve was always adopted. However, in practice most Codes allow a permissible grading curve region. The ideal Fuller curve is close to the lower boundary of this area.

To study the influence of the grading curve a curve is chosen which approximates the upper limit given in the Netherlands Code of Practice, the VB'74, for  $D_{max} = 32 \text{ mm}$  (Fig. 35).

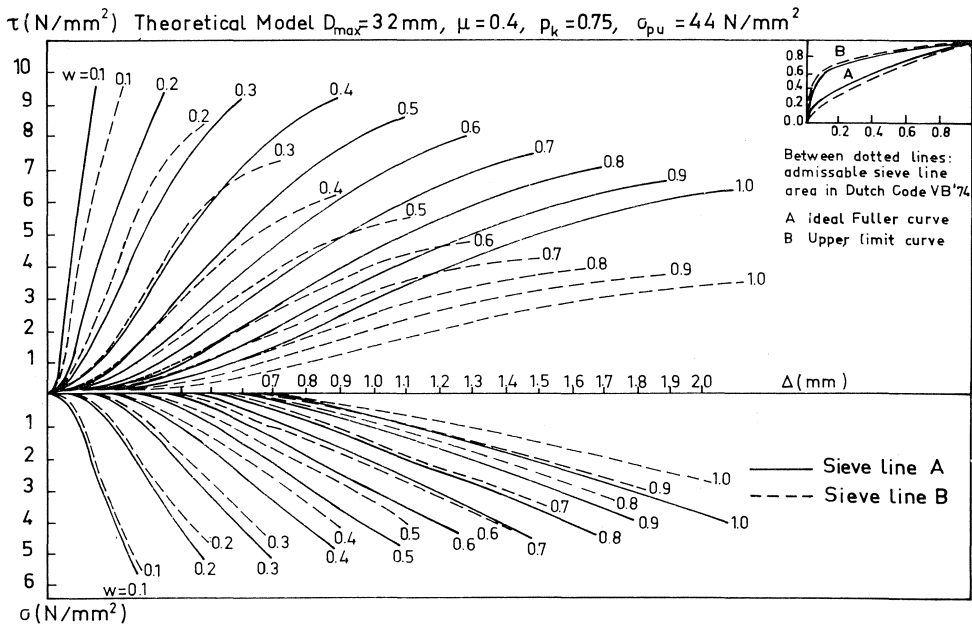


Fig. 35. The effect of the grading curve on the transfer of stresses in a crack for two comparable mixes, confirming to different grading curves ( $D_{max} = 32 \text{ mm}$ ,  $p_k = 0.75$ ,  $\sigma_{pu} = 44 \text{ N/mm}^2$ ,  $f_{cc} \approx 32 \text{ N/mm}^2$ )

The relations between stresses and displacements for the concrete conforming to the grading curve B in Fig. 35 were calculated. Other values adopted for  $D_{\max} = 16 \text{ mm}$  were  $p_k = 0.75$ ,  $\mu = 0.40$  and  $\sigma_{pu} = 44 \text{ N/mm}^2$ .

Although this concrete has the same maximum particle diameter  $D_{\max}$  as the comparable Fuller mix, it contains a much higher proportion of sand particles. The results previously obtained under b, where the contribution of the individual aggregate fractions to the transfer of stresses in a crack was established, were used for the calculations. The results for the concrete, designed with the grading curve B are represented in Fig. 35 by the dashed lines, and are compared with the results for the Fuller concrete calculated earlier (Fig. 34).

It is seen that in both cases the influence of the grading curve on the normal stresses  $\sigma$  is not great, but is significant for the shear stresses. The most pronounced differences are obtained for larger crack widths. This is to be expected, since the sandy mixes according to curve B provide a smaller potential contact area for larger crack width.

e. Cyclic loading:

From tests [43] it is known that in the case of cyclic loading a considerable difference exists between the behaviour of the crack plane during the first loading cycle and the subsequent cycles. The shear stress-shear displacement relationship of the initial cycle is almost linear, and after unloading a considerable amount of hysteresis can be observed. The shear stress-shear displacement relationship for the later loading cycles is highly non-linear, and a hardening type of behaviour is observed. This overall behaviour can be explained with the theory developed.

This is done on the basis of a fictitious specimen (Fig. 37) with a concrete quality of  $f_{cc} = 33.4 \text{ N/mm}^2$  and a maximum aggregate particle diameter of 32 mm, so that Fig. 31 can be used, a preset crack width of  $w_0 = 0.5 \text{ mm}$  and external restraint bars, providing an equivalent restraining stress of  $0.5 \text{ N/mm}^2$  for an increase of the crack width of 0.1 mm. The maximum shear stress applied is assumed to be  $\tau = 3 \text{ N/mm}^2$ . Fig. 36 shows the positions of the crack faces before and during loading.

When the shear load is increased, the crack faces engage in contact (Fig. 36b). The relation between  $\tau$  (shear stress) and  $\Delta$  (shear displacement) can be calculated using Fig. 31. If the maximum shear stress is reached (point A in Fig. 37b), the friction between particles and matrix is still a maximum ( $\mu = 0.40$ ). If the shear force is de-

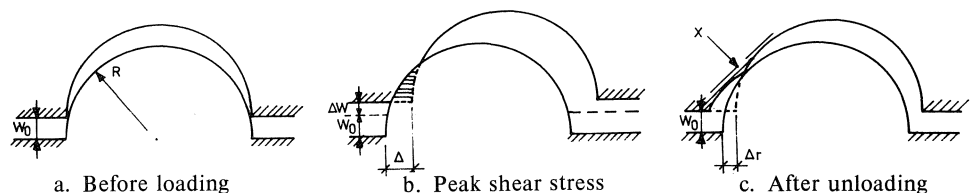
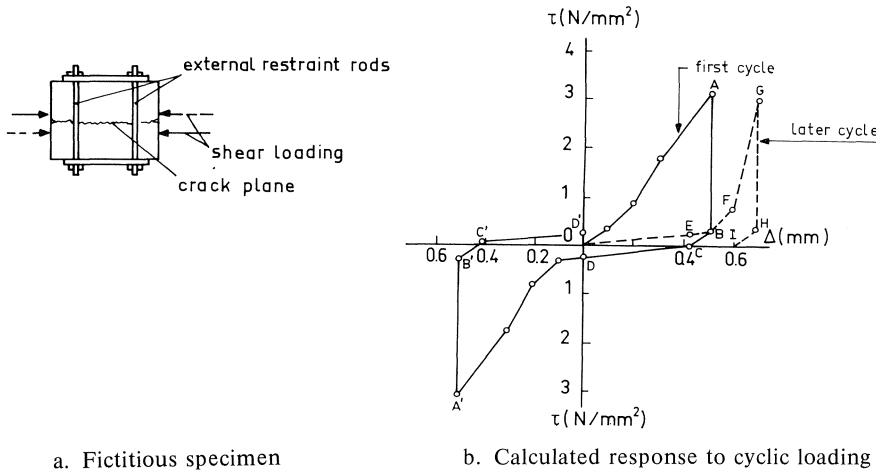


Fig. 36. Three characteristic stages during the first loading cycle.



a. Fictitious specimen                      b. Calculated response to cyclic loading

Fig. 37.

creased, relative movement between the crack faces can occur only if the maximum amount of friction in the opposite direction is exceeded. With the theoretical model it was calculated that this point is reached when the shear stress is reduced to  $0.24 \text{ N/mm}^2$  (point B in Fig. 37b). Fig. 36c shows that, after unloading, the “no contact phase” is reached before the shear displacement has returned to zero. The “no contact phase” is considered to be reached if in the most favourable case ( $R = \frac{1}{2}D_{\max}$ ,  $u = 0$ ) contact no longer exists. For the case considered it was calculated that the remaining shear displacement  $\Delta$ , is equal to  $0.41 \text{ mm}$  (point C in Fig. 37b). To restore the two halves of the specimen to their neutral position a small shear force may be necessary, since the “rubble” between the crack faces due to deterioration of matrix material during loading, may cause some frictional resistance (point D in Fig. 37b). If the shear force is applied in the other direction, the same type of behaviour can be expected, since those parts of the crack surfaces where contact occurs in this reversed cycle are not yet damaged (Fig. 36). Hence a similar loading and unloading curve can be expected (Fig. 37b, points A', B', C', D').

In the subsequent loading cycles the presence of the cavitations worn out in the first cycle of loading considerably affect the behaviour of the specimen. At first a shear displacement will occur at a small shear force, until contact between the opposing areas occurs ( $\Delta > 0.41 \text{ mm}$  (point E)). Then in a short interval of  $\Delta$  full contact between the cavities will be obtained. In this short interval a process of gradual wearing-off will occur at places of high contact stresses (point X in Fig. 36c). Hence a steeply ascending branch (EFG) may be expected, slightly shifted from the foregoing loading line. On unloading, behaviour similar to that in the first cycle may be expected (GHI - Fig. 37b).

A comparison of the  $\tau - \Delta$  relation based on the theoretical model, with experiments, carried out by Laible, White and Gergely [43], shows fairly good agreement in behaviour.

## 7 Analysis of the results of the tests with embedded bars

### 7.1 General

It appeared from the experimental results that the specimens with external restraint bars (Section 5) displayed a behaviour different from that of the specimens with embedded reinforcing bars (Section 4.1).

In the specimens with external bars the transmission of forces is completely governed by aggregate interlock. A larger restraint stiffness produces a steeper crack opening path. This could be physically explained (Chapter 6) and is also reflected in the diagrams, represented in the Figs. 17-20 (a higher value of  $r$  is attended with a greater shear displacement  $\Delta$  at the same crack width  $w$ ).

In the specimens with embedded bars a variation of the restraint stiffness generally did not affect the crack opening path. For values of the reinforcement ratio between 0.56-3.34% similar paths were obtained. Specimens in which soft sleeves were secured around the bars (Section 4.2) behaved in the same way as the specimens with external bars.

Hence it can be concluded that the existence of invariant crack opening paths is closely related to the presence of bond stresses. This could be explained by the fact that the high bond resistance of deformed bars causes a reduction of the crack width in the direct vicinity of the bars, whereas smooth bars generally result in an approximately constant crack width (Fig. 38).

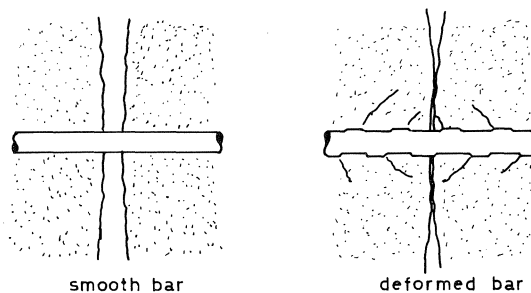


Fig. 38. Cracks for different types of bars.

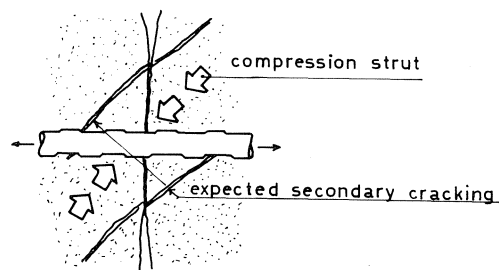


Fig. 39. Expected additional cracking for the case of deformed bars and shear loading.

With shear loading, high stresses occur in the region where the crack width is small (small crack widths are attended with high shear resistance, and, as a result, attract high stresses). Hence secondary cracking may occur around the bars, resulting in an additional mechanism: diagonal struts are formed, which force the crack faces to follow an opening path different from that which would be expected purely on the basis of the aggregate interlock mechanism (Fig. 39).

## 7.2 Components involved in the transmission of forces

During the transmission of forces across reinforced cracks a number of individual components are active that will be considered first:

### a. Aggregate interlock

Information on this action has already been given in Chapters 5 and 6.

### b. Axial restraint forces in the reinforcement

The relations between the axial forces in the reinforcing bars and the slip can be obtained by using a finite difference method, as proposed by Rehm [95] and Martin [97]. For this method the reinforcing bar is divided into elements with a length  $\Delta x$ .

Equilibrium of forces (Fig. 40)

$$\frac{d\sigma_s}{dx} = \frac{u}{A_s} \cdot \tau_x \quad (20)$$

In this equation  $u$  is the circumference of the reinforcing bar and  $A_s$  is the cross-sectional area; compatibility of deformations:

$$\frac{d\Delta x}{dx} = \frac{\sigma_{sx}}{E_s} \left( 1 - \frac{\sigma_{cx}}{\sigma_{sx}} \cdot \frac{E_s}{E_c} \right) \quad (21)$$

The basic load-slip relation, as obtained in experiments:

$$\frac{\tau}{f_{cc}} = a_0 + b_0 \Delta_s^{1/\beta} \text{ (cm)} \quad (22)$$

where  $a_0$ ,  $b_0$  and  $\beta$  are constants, which can be taken from Table 7.1.

Table 7.1 Constants in basic bond stress-slip relation (22) according to [97]

$f_R$	$a_0$	$b_0$	$\beta$
0.005	0.0320	0.129	2.34
0.010	0.0317	0.300	2.00
0.025	0.0317	0.680	1.85
0.050	0.0314	0.872	2.10
0.100	0.0315	1.135	2.31
0.200	0.0322	1.353	2.53
0.400	0.0316	1.308	2.85

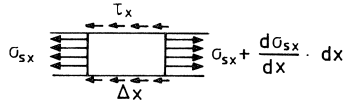


Fig. 40. Equilibrium of forces in a bar element.

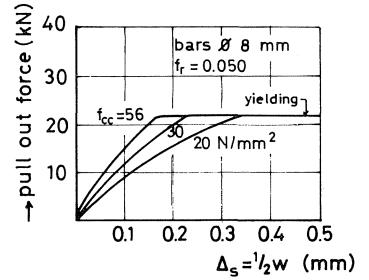


Fig. 41. Pull-out characteristic, calculated with the difference method.

The value  $f_R$  depends on the profiling of the bars. Average values for conventional steel bars are

$$\begin{aligned} f_R &\approx 0.045 \rightarrow 0.060 & \text{for } \varnothing = 4 \rightarrow 11 \text{ mm} \\ f_R &\approx 0.065 & \text{for } \varnothing > 12 \text{ mm} \end{aligned}$$

Fig. 41 shows a result of a pull-out characteristic, calculated with the difference method.

### c. Dowel action

The relation between dowel force and displacement can be approximately described by the model of a beam on an elastic foundation. For the case where no axial force is acting and the influence of the crack width as free length is neglected, the dowel force can be expressed as:

$$F_d = \beta^3 EI \cdot 2y_0 = \beta^3 EI \cdot \Delta \quad \text{with } \beta = \sqrt[4]{\frac{\varnothing G_f}{4EI}} \quad (23)$$

in which  $\Delta$  is the total shear displacement between the crack faces,  $I$  is the moment of inertia of the bar,  $G_f$  is the foundation modulus of the concrete. Substitution of

$$I = \frac{\pi \varnothing^4}{64}$$

results in

$$F_d = 3.56 \varnothing^{1.75} G_f^{0.75} \Delta \quad (24)$$

Tests by several authors [18, 64, 71] demonstrated that  $G_f$  does not depend on the bar diameter  $\varnothing$ . In experiments by Paulay [64], carried out with a constant concrete quality of  $f_{cc} \approx 30 \text{ N/mm}^2$ , the value of  $G_f$  was found to be a decreasing function of  $\Delta$ . A comparison of (24) with these experimental relations results in an expression for  $G_f$ :

$$G_f = 188 \Delta^{-0.85} \quad (25)$$

However,  $G_f$  must also be a function of the concrete strength. Because the modulus of elasticity  $E_c$  is generally related to the concrete strength according to:

$$E_c = C_1 \sqrt{f_{cc}}$$

a similar relation has been adopted for the foundation modulus:

$$G_f = C_2 \sqrt{f_{cc}}$$

Using this relation, equation (25) is modified to

$$G_f = 34 \sqrt{f_{cc}} \Delta^{-0.85} \quad (26)$$

This relation, however, is only based on experiments without axial tensile forces in the bars, i.e., for  $w = 0$ . Tests, carried out by Eleiott [18,88] showed that an axial tensile force in a bar reduces its dowel stiffness considerably: a tensile stress of  $175 \text{ N/mm}^2$  in a bar with  $\text{Ø}12.8 \text{ mm}$  reduced the dowel stiffness by about 50%, whilst an increase to  $350 \text{ N/mm}^2$  resulted again in a reduction of 40%. For the experiments in the authors' own program, a stress level of  $175 \text{ N/mm}^2$  is approximately obtained for a crack width of  $w = 0.2 \text{ mm}$  and a stress of  $350 \text{ N/mm}^2$  for  $w = 0.4 \text{ mm}$ . Taking these values into account, an approximate reduction factor can be formulated:

$$\xi = 0.20(w + 0.2)^{-1} \quad (27)$$

Combining (24), (26) and (27), an approximate estimation of the dowel force is obtained, taking into account the influence of crack width, shear displacement, bar diameter and concrete quality:

$$F_d = 10(w + 0.2)^{-1} \Delta^{0.36} \text{Ø}^{1.75} f_{cc}^{0.38} \quad (28)$$

On comparing the values obtained with (28) for the measured crack opening path with the total shear force in the experiments, it is seen that dowel action is of minor importance (Fig. 42).

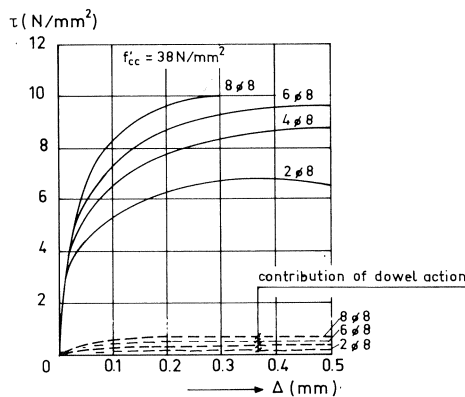


Fig. 42. Contribution of dowel action, calculated with equation (28), to the total shear stress in a crack, for the basic series made with concrete mix 5, reinforced with 2, 4, 6 and 8 stirrups  $\text{Ø}8 \text{ mm}$ .

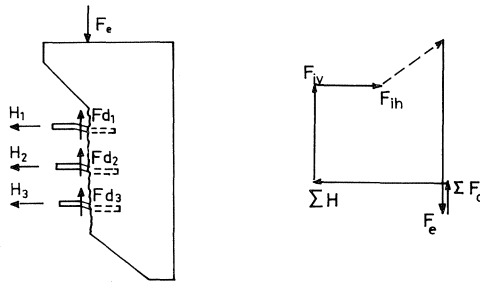


Fig. 43. Equilibrium of forces in a reinforced crack.

### 7.3 Analysis of test results

The individual components, namely, aggregate interlock, axial restraint stiffness, and dowel action, have previously been expressed as functions of the crack width  $w$  and the stress displacement  $\Delta$  of the crack faces. This makes possible a further analysis of the results of the tests on specimens with embedded bars.

In principle the equilibrium of a crack can be represented by a polygon of forces as shown in Fig. 43.

The external shear force  $F_e$  was measured by a load cell, the dowel force  $F_d$  can be calculated with equation (28), the axial restraint force  $H$  of the reinforcement normal to the crack plane can be calculated with the equations (20, 21, 22) and the aggregate interlock components can be calculated with the equations presented in Chapter 5. The additional mechanism which acts around the reinforcing bars (Fig. 39) provides a force that cannot be measured. This force is indicated in Fig. 43b as a dotted line, closing the polygon. This equilibrium has been studied for all specimens and for many ( $w, \Delta$ ) combinations. The following properties were found:

- If the reinforcement ratio was small (2 stirrups  $\text{Ø}8 = 0.56\%$  or smaller), the dotted “closing line” was not necessary to provide equilibrium.
- Hence in this case the specimens behaved in the same way as the specimens with external restraint bars.
- If the reinforcement ratio was greater, the “closing line” was always perpendicular to the actual crack opening direction ( $d\Delta/dw$ ).

To be able to describe the behaviour of the reinforced specimens the model shown in Fig. 44 was adopted. In this model the following components are active:

- $F_s$ : spring, representing the restraining action of the reinforcement
- $F_d$ : dowel action of the reinforcement
- $F_{ih}, F_{iv}$ : Springs, representing the horizontal and vertical action of aggregate interlock
- $s$ : Infinitely stiff rotating strut, representing the effect of the additional mechanism around the reinforcing bars (Fig. 39). The strut can only be loaded in compression. The direction is dependent on the critical crack

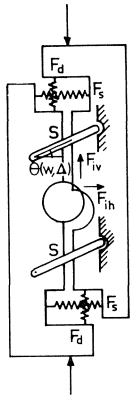


Fig. 44.  
Schematic representation of forces  
in a reinforced crack.

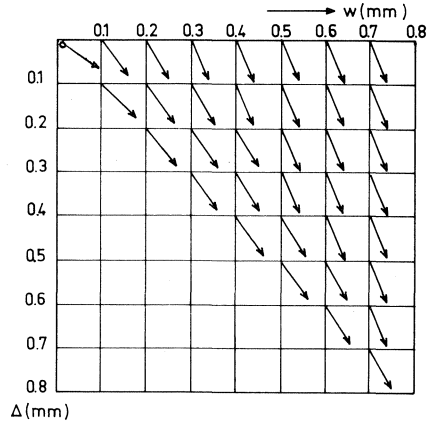


Fig. 45.  
Critical crack opening directions  
according to eq. 29.

opening direction. It is assumed that for every  $(w, \Delta)$  combination a critical crack opening direction exists. If  $dw \gg d\Delta$ , no additional “locking up” of the crack faces around the bars occurs; if  $d\Delta \gg dw$ , “locking up” occurs, resulting in high stress concentrations, which in turn activate the “strut action”.

On the basis of the experimental results of this project and the results reported by Mattock [53], who also found “critical directions” starting from larger initial crack widths, the critical crack opening direction for concrete mixtures having moderate strengths (characterized by the property that the cracks run in general along the circumference of the aggregate particles and do not intersect them) was formulated as follows:

$$\frac{d\Delta}{dw} = w^{0.18}(1.65 + 2.10w) - 1.5\Delta \quad (29)$$

With this formula all the results available at the moment were satisfactorily predictable. A few examples are given in Figs. 46 and 47.

Fig. 46 shows the results of a series of tests on specimens with a cube compressive strength  $f_{cc} = 30 \text{ N/mm}^2$ , with reinforcement ratios ranging from 0.56% to 2.24%. It is seen that in three cases a good prediction is obtained. Only in the case of the high reinforcement ratio (8 stirrups  $\text{Ø}8 \text{ mm}$ ) was the actual curve lower than the predicted one. This can be explained by the observation that some spalling of concrete occurred in the top and bottom area of the crack, so that the actual shear plane was reduced. This spalling is probably caused by the circumstance that the stress combinations are not completely uniform along the crack and less favourable combinations are found at the ends of the crack. This type of spalling was found only for high reinforcing ratios and low concrete strengths ( $f_{cc} < 30 \text{ N/mm}^2$ ). It turned out that specimens of the type represented in Fig. 1a are more sensitive to this phenomenon than the others. It must be empha-

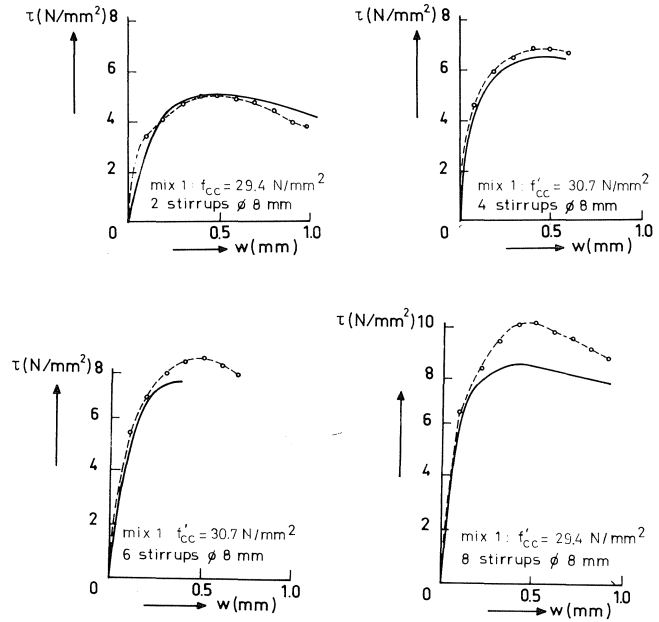


Fig. 46. Comparison between experimental and calculated curves for specimens made of mix No. 1 (Section 4.1), with  $f_{cc} = 30 \text{ N/mm}^2$  and varying reinforcement ratios.

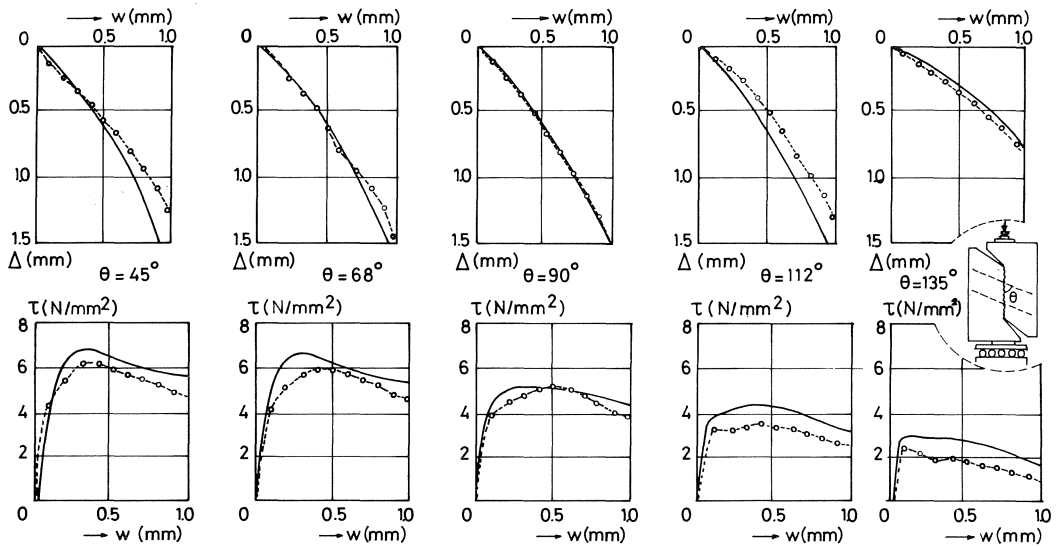


Fig. 47. Comparison between calculated (dotted) and experimental (solid)  $\tau - w$  and  $w - \Delta$  relations for specimens with inclined bars.

sized that, when interpreting test results, such effects should always be taken into account.

Fig. 47 gives a comparison between the experimental and the calculated curves for the tests on specimens with inclined bars. Further analysis of reinforced cracks is necessary. It should be investigated whether the existence of critical crack opening directions is dependent on the profiling of the steel: smooth bars will not reduce the crack width around the bars to such an extent as deformed bars will.

Furthermore it would be useful to carry out tests on specimens, subjected to both shear and tension normal to the crack: The advantage of such tests is that the crack opening path can be varied, so that any  $(w, \Delta)$  can be obtained. Also, the influence of load history can be studied in such a way.

In [94] it is shown how the relations, based on the behaviour of reinforced cracks as observed in this project, can be used for constitutive relations for cracked reinforced concrete.

## 8 A model for the behaviour of cracked reinforced concrete

It is endeavoured to formulate the relation between stresses and strains of cracked reinforced concrete on the basis of existing knowledge. Use is made of an earlier proposal made by Bazant and Gambarova [98], which is extended with regard to the crack properties, the development of the crack pattern and tension stiffening.

### 8.1 The stress-displacement relation for a single crack

A distinction has to be made between the two cases of a crack in plain concrete and a crack in reinforced concrete. The experiments demonstrated that in the case of reinforced cracks the crack opening direction may be confined to a certain limit value. To simulate the behaviour displayed by the cracks a compression strut has been introduced (Fig. 44), which is activated only if the shear displacement tends to exceed the limit value.

#### a. The unreinforced crack

For the sake of succinct formulation a modified notation is used for the stresses and displacements, referring to the directions  $n$  (normal to the crack) and  $t$  (tangential to the crack) (Fig. 48).  $\delta_n$  and  $\delta_t$  represent the displacements in the normal and tangential directions ( $\delta_n > 0$ :  $\delta_n$  = crack width, earlier denoted as  $w$ ),  $\delta_t$  = shear displacement (earlier denoted as  $\Delta$ ). The associated stresses are  $\sigma_{nn}$  (normal stress) and  $\sigma_{nt}$  (shear stress).

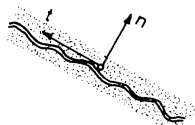


Fig. 48. Principal directions  $n$  and  $t$ .

The relations between  $\sigma_{nn}$ ,  $\sigma_{nt}$  and  $\delta_{nn}$ ,  $\delta_{nt}$  can be expressed as:

$$\begin{Bmatrix} d\sigma_{nn} \\ d\sigma_{nt} \end{Bmatrix} = \begin{bmatrix} B_{nn} & B_{nt} \\ B_{tn} & B_{tt} \end{bmatrix} \begin{Bmatrix} d\delta_n \\ d\delta_t \end{Bmatrix} \quad \text{or} \quad \{d\sigma\} = [B^{cr,p}]\{d\delta\} \quad (30)$$

where  $B_{nn}$ ,  $B_{nt}$ ,  $B_{tn}$  and  $B_{tt}$  are the crack stiffness coefficients: the superscripts cr, p refer to crack and plain concrete. With the equations (1a) and (1b) simplified expressions have been given for the relations between  $\sigma_{nn}$ ,  $\sigma_{nt}$  and  $\delta_{nn}$ ,  $\delta_{nt}$ . In a generalized way these functions are represented by

$$\sigma_{nn} = f_n(\delta_n, \delta_t), \quad \sigma_{nt} = f_t(\delta_n, \delta_t) \quad (31)$$

Differentiation of (31) results in expressions for the crack stiffness coefficients:

$$B_{nn} = \frac{\partial f_n}{\partial \delta_n}, \quad B_{nt} = \frac{\partial f_n}{\partial \delta_t}, \quad B_{tn} = \frac{\partial f_t}{\partial \delta_n}, \quad B_{tt} = \frac{\partial f_t}{\partial \delta_t} \quad (32)$$

These relations are valid for increasing values of  $\delta_n$  and  $|\delta_t|$ , as generally encountered in the case of monotonically increased loading. A path-dependent formulation, taking into account plastic deformations and friction between particles and matrix, would be possible on the basis of the data presented in the Chapters 5 and 6, but would require more complicated expressions. Considering the values of the crack stiffness coefficients, it can be expected that the crack stiffness matrix is not positive definite. However, the unstable behaviour is usually stabilized by the restraint provided by the reinforcement and the boundary conditions [98].

#### b. The reinforced crack

A distinction has to be made between the case where the crack opens freely and the case where crack opening is confined to a limit direction due to secondary effects caused by local modifications of the crack structure around the reinforcing bars due to splitting forces. In Fig. 44 it was shown that in the case of a confined crack opening it is possible to simulate the behaviour by the introduction of hinged struts with high stiffness. The direction of the struts depends on the actual combination of displacements ( $\delta_n$ ,  $\delta_t$ ) Fig. 49).

The relation between stresses and displacements is now of function of two mechanisms: the compression struts and the particle-matrix interaction, as formulated in section 8.1a. In the following formulation the influence of dowel action is neglected.

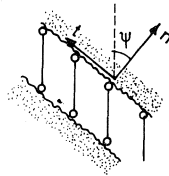


Fig. 49. Compression struts as an expedient to simulate the behaviour of reinforced cracks.

The average stresses, caused by the very stiff compression struts, are represented by

$$\{d\sigma^{\text{str}}\} = [B^{\text{str}}]\{d\delta^{\text{cr}}\} \quad (33)$$

where the superscript str refers to strut and cr refers to crack. Since the struts are inclined to the crack, the matrix  $[B^{\text{str}}]$ , which is by definition related to the crack direction  $(n, t)$ , has to be obtained by the transformation

$$[B^{\text{str}}] = [R^{\text{str}}]^T [B_{\psi}^{\text{str}}] [R^{\text{str}}] \quad (34)$$

with

$$[R^{\text{str}}] = \begin{bmatrix} M^2 & 2MN \\ -MN & M^2 - N^2 \end{bmatrix}$$

and

$$[B_{\psi}^{\text{str}}] = \begin{bmatrix} E_{\text{str}} & 0 \\ 0 & 0 \end{bmatrix}$$

where  $M = \cos \psi$ ,  $N = \sin \psi$  and  $\psi$  is the angle between the direction normal to the crack and the direction of the struts. The direction of the struts depends on the combination of displacements:  $\psi = \psi(\delta_n, \delta_t)$  (29).

A sufficiently high stiffness could be attributed to the struts. The stresses in the crack as a result of the particle-matrix interaction have earlier been formulated in equation (30). Summation of the stresses caused by both effects yields

$$\{d\sigma^{\text{cr}}\} = [B^{\text{cr},r}]\{d\delta^{\text{cr}}\} \quad (35)$$

with

$$[B^{\text{cr},r}] = [B^{\text{cr},p}] + [B^{\text{str}}] \quad (36)$$

where the superscript cr,r refers to crack in reinforced concrete. If the struts are subjected to tensile forces, the matrix  $B^{\text{str}}$  is defined to be  $[B^{\text{str}}] = [0]$ .

## 8.2 The relation between stresses and displacements in cracked reinforced concrete

A cracked concrete element is considered, reinforced with steel bars in one direction. The concrete is intersected by a system of parallel cracks of average spacing  $s$ ; the angular deviation between the bars and the crack normal is equal to  $\theta$  (Fig. 50).

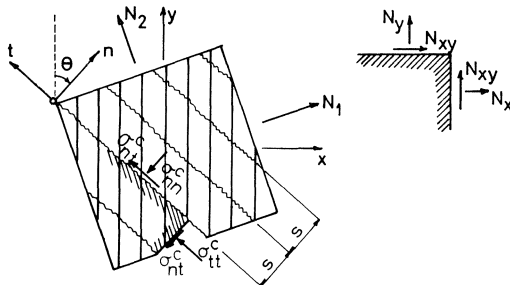


Fig. 50. Reinforced concrete element intersected by cracks [98].

It is assumed that the element is sufficiently large compared to the spacing of bars and cracks and that the internal forces vary gradually and smoothly, so that they could be assumed to be almost uniform over a distance of several bar and crack spacings. By inversion of the crack stiffness matrix  $[B^{cr,\Gamma}]$  from equation (36), we obtain:

$$\begin{Bmatrix} d\delta_n \\ d\delta_t \end{Bmatrix} = \begin{bmatrix} F_{nn} & F_{nt} \\ F_{tn} & F_{tt} \end{bmatrix} \begin{Bmatrix} d\sigma_{nn} \\ d\sigma_{nt} \end{Bmatrix} \quad (37)$$

or

$$\{d\delta^{cr}\} = [F^{cr,\Gamma}]\{d\sigma^{cr}\}$$

where  $[F^{cr,\Gamma}]$  is the flexibility matrix of the crack and  $[F^{cr,\Gamma}] = [B^{cr,\Gamma}]^{-1}$ .

The average strains resulting from the “smeared out” cracks are:

$$\varepsilon_{nn}^{cr} = \frac{\delta_{nn}}{s(\varepsilon)}, \quad \gamma_{nt}^{cr} = 2\varepsilon_{nt}^{cr} = \frac{\delta_{nt}}{s(\varepsilon)} \quad (38)$$

The superscript cr indicates that only deformations directly related to the crack displacements are considered.  $s(\varepsilon)$  is the mean crack spacing attended by a strain condition  $\{\varepsilon\}$ . The mean crack spacing  $s(\varepsilon)$  depends on a number of influencing factors:

- the bond-slip relation, depending on the profiling of the reinforcing bars, the concrete quality and the stresses in the surrounding concrete;
- geometrical effects, such as the bar diameter, bar spacing and concrete cover;
- the concrete tensile strength (low strength results in many cracks), which is also influenced by the stresses in the surrounding concrete due to external forces;

Concerning the crack pattern a number of formulations are known, mostly for cases where the reinforcement is perpendicular to the cracks. The average crack distance in a stabilized crack pattern, where no more cracks can be formed, is formulated by most investigators as

$$s_m = k_1 c + k_2 k_3 \frac{\emptyset}{\rho} \quad (39)$$

where  $c$  is the concrete cover and  $k_1, k_2, k_3$  are constants.

Table 8 I

Author	$k_1$	$k_2 k_3$	Remarks
Rehm/Martin [109]	1.5	0.10-0.14	$k_2 = \frac{0.9}{0.2 + f_R^{2/3}} 10^{-2}$ $k_3 = 5$ (for $f_R$ see Chapter 7.2)
Monterio [110]	1.5	0.16	
Ferry-Borges [111]	1.5	0.02-0.04	
Efsen [112]	2.5/c	0.17	
Beeby [113]	1.33	0.08	
Broms [103-106]	2.0	0	
Rostasy, Alda [114]	1.5	0.04-0.09	lightweight concrete

Table 8 II

Author	$k_4$
Ferry-Borges [111]	$0.75/(\rho\sigma_{s,cr})$
Monterio [111]	$3/(\rho\sigma_{s,cr})$
Falkner [115]	$1/2f_{ct}/(\rho\sigma_{s,cr})$
Rostasy, Koch, Leonhardt [116]	$\left\{ \frac{f_{ct}}{\rho} \right\}^2 \frac{(1+n\rho)}{(\sigma_{s,cr})^2}$
Leonhardt [117, p. 22]	$\left\{ \frac{f_{ct}}{\rho\sigma_{s,cr}} \right\}^2$

$k_1$  = associated with the distance necessary to attain a uniformly distributed stress distribution

$k_2$  = depends on the profiling of the steel

$k_3$  = depends on the loading case (tension, flexure)

A survey of the values for  $k_1$  and  $k_2k_3$  for pure tension, given by a number of investigators, is presented in Table 8 I.

The average crack width for a stabilized crack pattern can be obtained with the aid of eq. (39)

$$w_m = s_m \frac{\sigma_{s,cr} - \Delta\sigma_s}{E_s} = s_m \frac{\sigma_{s,cr}}{E_s} (1 - k_4) \quad (40)$$

where  $\sigma_{s,cr}$  is the steel stress in a crack, and  $\Delta\sigma_s$  is a term taking account of the fact that the steel stress in the uncracked concrete over the transmission length of the bond stresses is lower than in the crack itself, which has a reducing influence on the crack width. For the constant  $k_4$  several expressions are found (Table 8 II).

Dynamic loading and long-term loading have a reducing effect on the term  $k_4$ . Leonhardt [117] indicates that, depending on the load intensity or loading time, the value  $k_4$  is reduced to 80–40% of the initial value. Experiments by Straninger [118], subjecting centrally reinforced concrete prisms to long term loading, displayed a reduction to about 60%. This is in good agreement with the value 50%, given by CEB [119].

Leonhardt [117] indicates further that in the case of centric tension, under the maximum service load, the increase of crack width can amount up to 20%.

By formula (40) the average crack width is determined for the case of a stabilized crack pattern. The amount of scatter in crack width found may be of interest. Several investigators give information on this, mostly expressed by the ratio  $w_{95\%}/w_m$ . A survey is given in Table 8 III.

The semi-empirical formula (39) gives only the average crack spacing for a stabilized crack pattern. To formulate the stress-strain relations for cracked reinforced concrete it is necessary to know the number of cracks, or the average spacing, in the loading state

Table 8 III

Author	$w_{95\%}/w_m$	$w_{99\%}/w_m$	$w_{max}/w_m$	statistical distribution
Clark [120]	1.64			normal
Kaar/Mattock [121]	1.3-1.5			normal
Ferry-Borges [111]	1.66			normal
Beeby [113]	1.4			oblique
Broms [106]			2	normal
Base [107]		2		normal

between the first crack and the stabilized crack pattern. Only a few investigators give information on this.

For the crack spacing Efsen [112] gives a relation similar to eq. (39):

$$s_m = k_1 + 0.25k_2 \frac{\varphi}{\rho}$$

where  $k_1$  and  $k_2$  depend on  $\sigma_{s,cr}$  (Fig. 51).

A stabilized crack pattern is obtained for  $\sigma_{s,cr} = 400 \text{ N/mm}^2$ , giving  $0.25k_2 = 0.17$  and  $k_1 = 25 \text{ mm}$ , which is in good agreement with the values from Table 8 I. However, the assumption that the crack pattern is stabilized reaching  $\sigma_{s,cr} = 400 \text{ N/mm}^2$  is not always in agreement with experimental observations. Rostasy and Alda [114] show that the degree of development of the crack pattern greatly depends on the reinforcing ratio. It was calculated that for a yield stress of  $420 \text{ N/mm}^2$  and low values of  $\rho$ , the cracking pattern was only half developed at reaching this yield stress, whilst for higher values of  $\rho$  the cracking pattern was stabilized long before.

Schäfer [69, pp. 123, 124] gave a pragmatic approach of the development of crack distance and crack width, basing himself on the equations (39) and (40).

To make allowance for load history, eq. (39) is extended in that for the first cracking load  $s = \infty$  is found whilst on further loading a rapid approach to the values of (39) is obtained:

$$s(\varepsilon_{nn}) = \frac{\varepsilon_{cr} + \varepsilon_{nn}}{\varepsilon_{nn} - \varepsilon_{cr}} \cdot s_m \quad (41)$$

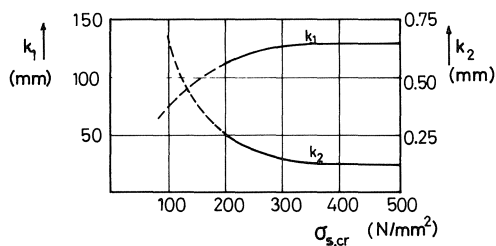


Fig. 51.

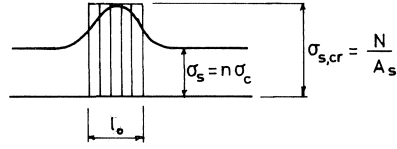


Fig. 52.

where  $\varepsilon_{cr}$  is the strain at which the first crack occurs (suggested value  $s = 0.0001$ ) and  $\varepsilon_{nn}$  is the average strain normal to the crack. The crack width was formulated as

$$w(\varepsilon_{nn}) = \frac{\varepsilon_{nn} - \varepsilon_{cr}}{\varepsilon_{nn} + \varepsilon_{cr}} \cdot w_m \geq 0 \quad (42)$$

These equations were compared with experimental values (Peter, [121]): it appeared that a good prediction for the transition range between uncracked and completely cracked (stabilized) was possible. However, probably the same objection as raised to Efsen formulations applies here.

Rostasy and Alda [114] gave a method, based on a technique introduced by Falkner [115]. This technique implies that the element is divided into smaller parts. To get a simple model for each crack a fictitious length  $l_0$  is defined, over which bond is completely destroyed (Fig. 52).

For a stabilized crack pattern  $w_m = s_m \cdot \varepsilon_{nn}$  or  $w_m = l_0 \varepsilon_{s,cr}$ . On the assumption that, during the formation of new cracks, the external tensile force does not exceed the first crack load, Falkner gives

$$l_0 = s_m \frac{\varepsilon_{nn}}{\varepsilon_{s,cr}} = s_m \left( 1 - \frac{k_4}{f_{ct}} \right) \quad (43)$$

where  $k_4$  can be taken from Table 8 II. With this method the strain of a centrally reinforced element, subjected to a tensile force  $N_{cr}^m$  (external force at which the  $m^{\text{th}}$  crack occurs), can be derived from the behaviour of a series of springs:

$$\varepsilon_{nn} = \frac{N_{cr}^m}{E_c \cdot A_i} \cdot \frac{1}{l} (l - ml_0) + \frac{N_{cr}^m}{E_s A_s} \frac{ml_0}{l} \quad (44)$$

with  $A_i = A_c(1 + n\rho)$ ,  $m$  = number of cracks,  $l$  = length of the element perpendicular to the cracks,  $n = E_s/E_c$ .

The number of cracks can then be formulated as

$$m(\varepsilon_{nn}) = \frac{E_c A_i \varepsilon_{nn} - N_{cr}^m}{N_{cr}^m} \cdot n\rho \frac{l}{l_0} \quad (45)$$

The crack pattern is stabilized when  $s_m$  is reached. The maximum number of cracks is  $m = l/s_m$ .

Rostasy, Koch, Leonhardt [116], taking account of the effect of tension stiffening, give the relation

$$\frac{\varepsilon_{nn}}{\varepsilon_{s,cr}} = 1 - \left\{ \frac{f_{ct}}{\rho} \right\}^2 \frac{(1+n\rho)}{(\sigma_{s,cr})^2} \quad (46)$$

(see also Table 8 II). Substitution of (46) into (45) gives the relative number of cracks

$$\frac{m(\varepsilon_{nn})}{m} = \frac{s_m}{l_0} \left[ \frac{2(1+n\rho)}{1 + \sqrt{1 + \frac{4}{1+n\rho} \left( \frac{\varepsilon_{cr}}{\varepsilon_{nn}} \right)^2 \left( \frac{1+n\rho}{n\rho} \right)^2}} - n\rho \right] \leq 1 \quad (47)$$

with  $\varepsilon_{cr}$  = concrete strain at cracking.  $s_m/l_0$  is obtained from (43)

Because of the relation

$$s_m(\varepsilon_{nn}) = s_m \frac{m(\varepsilon_{nn})}{m} \quad (48)$$

it is possible to calculate directly from (47) the average crack spacing relating to an arbitrary value of  $\varepsilon_{nn}$ .

Since  $s_m(\varepsilon_{nn})$  is known, a combination of (37) and (38) gives:

$$\begin{Bmatrix} d\varepsilon_{nn}^{cr} \\ d\varepsilon_{tt}^{cr} \\ dy_{nt}^{cr} \end{Bmatrix} = \begin{Bmatrix} F_{nn} s_m^{-1}(\varepsilon_{nn}) & 0 & F_{nt} s_m^{-1}(\varepsilon_{nn}) \\ 0 & 0 & 0 \\ F_{tn} s_m^{-1}(\varepsilon_{nn}) & 0 & F_{tt} s_m^{-1}(\varepsilon_{nn}) \end{Bmatrix} \begin{Bmatrix} d\sigma_{nn}^c \\ d\sigma_{tt}^c \\ d\sigma_{nt}^c \end{Bmatrix} \quad (49)$$

which may be written in abridged form as:

$$\{d\varepsilon^{cr}\} = [D^{cr}]\{d\sigma^c\} \quad (50)$$

Here the superscript  $c$  refers to the concrete between the cracks. The last equation indicates that the stresses in the concrete are equal to those in the cracks. The average strains of the cracked reinforced concrete element  $\varepsilon_{nn}$ ,  $\varepsilon_{tt}$  and  $\gamma_{nt}$  can be obtained as the sums of the strains of the solid concrete between the cracks  $\varepsilon_{nn}^c$ ,  $\varepsilon_{tt}^c$  and  $\gamma_{nt}^c$  and the strains due to the cracks  $\varepsilon_{nn}^{cr}$ ,  $\varepsilon_{tt}^{cr}$ ,  $\gamma_{nt}^{cr}$ ; so

$$\{d\varepsilon\} = \{d\varepsilon^{cr}\} + \{d\varepsilon^c\} \quad (51)$$

where  $\{d\varepsilon\} = (d\varepsilon_{nn}, d\varepsilon_{tt}, dy_{nt})^T$ ,  $T$  denoting the transpose, and  $\{d\varepsilon^{cr}\}$ ,  $\{d\varepsilon^c\}$  are the analogous column matrices for strains due to cracks and to concrete between the cracks. The strains in the concrete between the cracks are related to the stresses by the incremental stress-strain relation

$$\{d\varepsilon^c\} = [D^c]\{d\sigma^c\} \quad (52)$$

where  $D^c$  is the tangent flexibility matrix of concrete. Substitution of (50) and (52) into (51) yields

$$\{d\varepsilon\} = [D]\{d\sigma^c\} \quad [D] = [D^{cr}] + [D^c] \quad (53)$$

where  $D$  is the flexibility matrix of cracked concrete as a whole. Equation (53) being known, the influence of the reinforcement can be inserted. It is assumed that the average strains of the reinforcement are equal to those of the cracked concrete. The effect of tension stiffening is implied in the stress-strain relation of the steel. The averaged stresses are:

$$\{d\sigma^s\} = [C^s]\{d\varepsilon\} \quad (54)$$

where the superscript  $s$  refers to steel. Since the cracks are in general inclined with respect to the reinforcing bars, the matrix  $[C^s]$ , which is by definition related to the axes  $n$  and  $t$ , must be obtained by the transformation:

$$[C^s] = [R^s]^T [C_\theta^s] [R^s]$$

$$[R^s] = \begin{bmatrix} P^2 & Q^2 & 2PQ \\ Q^2 & P^2 & -2PQ \\ -PQ & PQ & P^2 - Q^2 \end{bmatrix} \quad (55)$$

with

$$[C_\theta^s] = \begin{bmatrix} \alpha\rho_\theta E_s(\varepsilon) & 0 & 0 \\ 0 & 0 & 0 \\ 0 & 0 & 0 \end{bmatrix} \quad (56)$$

where  $P = \cos \theta$ ,  $Q = \sin \theta$ ,  $\theta$  is the angle between the reinforcing bars and the direction normal to the crack (Fig. 50).  $E_s(\varepsilon)$  is the tangential spring stiffness of the reinforcing steel,  $\rho_\theta$  is the reinforcing ratio in the bar direction, and  $\alpha$  is a factor taking account of the effect of tension stiffening.

The coefficient  $\alpha$  can be derived from the general relations representing the effect of tension stiffening.

$$\frac{\varepsilon_{nn}}{\varepsilon_{s,cr}} = 1 - k_4 \quad (57)$$

(for  $k_4$  see Table 8 II).

If, for instance, the value, suggested by Leonhardt, Koch, Rostasy is inserted, we obtain:

$$\varepsilon_{nn} = \varepsilon_{s,cr} \left\{ 1 - \frac{f_{ct}^2}{\rho^2 \sigma_{s,cr}^2} (1 + n\rho) \right\} \quad (58)$$

Substitution of

$$\varepsilon_{s,cr} = \frac{\sigma_{s,cr}}{E_s} = \frac{\sigma_{nn}}{\rho E_s}$$

in (58) and differentiation with respect to  $\sigma_{nn}$  yields:

$$d\sigma_{nn} = \frac{\rho E_s}{1 + f_{ct}^2 (1 + n\rho) \sigma_{nn}^{-2}} \cdot d\varepsilon_{nn}$$

so that

$$\alpha = \frac{1}{1 + f_{ct}^2(1 + n\rho)\sigma_{nn}^{-2}} \quad (59)$$

Finally the stresses due to the cracked concrete and to the steel bars must be added:

$$\{d\sigma\} = \{d\sigma^c\} + \{d\sigma^s\}$$

Because, according to equation (53):

$$\{d\sigma^c\} = [D]^{-1}\{d\varepsilon\}$$

this results in

$$\{d\sigma\} = [C]\{d\varepsilon\} \quad \text{with} \quad [C] = [C^s] + [D]^{-1}$$

where  $[C]$  is the tangential stiffness matrix of cracked reinforced concrete, referred to the axes  $n$  and  $t$ . This matrix  $[C]$  must of course be further transformed to the element coordinates.

## 9 Conclusions

1. Shear transfer across cracks cannot be simply formulated as a relation between shear stress and shear displacement, but is a more complex mechanism, in which shear stress, shear displacement, normal stress and crack width are involved.
2. In cracks in plain concrete the stresses in the normal and the shear direction are mainly a function of crack width, shear displacement and concrete quality.
3. The mechanism of aggregate interlock can be adequately described on the basis of the behaviour at micro-level, in which sliding friction between particles and matrix and irreversible deformation of the matrix are the essential mechanisms.
4. The normal and shear stresses in unreinforced cracks in any concrete can be adequately described by simple mathematical functions of crack width, shear displacement and concrete strength (for monotonic loading).
5. There is a fundamental difference between the behaviour of reinforced cracks and unreinforced cracks which are restrained by external bars. Whereas the crack opening path for reinforced cracks is approximately constant, irrespective of the reinforcement ratio, it depends clearly on the external restraint stiffness for cracks in plain concrete. This difference in behaviour is probably caused by the reduction of the crack width around the bars due to bond stresses.
6. The crack opening path (relation crack width – shear displacement) for reinforced cracks subjected to shear loading is not influenced by variation of the reinforcement ratio between 0.6–3.4% for the same concrete quality. The differences between the crack opening paths for various concretes with moderate strengths (20–38 N/mm<sup>2</sup>) are negligible. Steeper crack opening paths (shear displacement large with regard to crack opening in the normal direction) are observed in concretes in which the crack intersects a number of the aggregate particles.

7. Variation of bar diameters in reinforced cracks, while the reinforcement ratio remains constant, has no significant influence on the behaviour.
8. Variation of the aggregate composition by increasing the size of the aggregate (maximum aggregate particle 32 mm instead of 16 mm, or by removing all aggregate particles between 0.25 and 1.00 mm) does not significantly influence the behaviour.
9. The normal and shear displacements in reinforced cracks subjected to an external shear force decrease with increasing reinforcement ratio and concrete strength. The ultimate resistance is increased by higher concrete strength.
10. Unloading and reloading of cracks gives rise to a considerable amount of hysteresis of the shear stress - shear displacement relations, indicating the presence of frictional action.

## 10 Notation

The most frequent symbols of this paper are:

$A$  = cross-sectional area

$D$  = particle size of aggregate

$f$  = strength

$w$  = crack width

$\Delta$  = shear displacement

$\rho = A_s/A_c$  = reinforcement ratio

$\sigma$  = normal stress

$\tau$  = shear stress

$\emptyset$  = bar diameter

### Subscripts

$c$  = concrete

$s$  = steel

$cc$  = concrete cube compression

$ct$  = concrete tension

$sy$  = steel yield

## 11 References

1. ACI-ASCE Committee 426, The shear strength of reinforced concrete members, Journal of the Structural Division, ASCE, V 99, No. ST6, June 1973, pp. 1091-1187.
2. ARROYO, J., Study of dowel action of the main reinforcement of reinforced concrete beams, Thesis, Imperial College, London, 1969.
3. BAUMANN, T. and H. RÜSCH, Versuche zum Studium der Verdübelungswirkung der Biegebewehrung eines Stahlbetonbalkens, Deutscher Ausschuss für Stahlbeton, Heft 210, Berlin, 1970.
4. BENNETT, E. W. and S. BANERJEE, Strength of beam column connections with dowel reinforcement, The Structural Engineer, Vol. 54, April 1976, No. 4, pp. 133-139.
5. BIRKELAND, P. W. and H. W. BIRKELAND, Connections in precast concrete constructions, ACI-Journal, Vol 63, No. 3, March 1966, pp. 345-368.
6. BRAESTRUP, M. W., Plastic analysis of shear in reinforced concrete, Report No. 70, Afdelingen for Baerende Konstruktioner, Technical University of Denmark, Kopenhagen, 1970.
7. Building Code Requirements for Reinforced Concrete (ACI 318-71), American Concrete Institute, Michigan, 1971.
8. CEB Bulletin d'Information No. 117, Vol. II, Model Code for Concrete Constructions, December 1976.
9. CEDOLIN, L. and S. DEI POLI, Non-linear plane stress analysis of reinforced concrete by the finite element method, Construzioni in cemento armato, Studi e Rendiconti, Politecnico di Milano, Vol. VIII, 1977, pp. 3-33.
10. CEDOLIN, L. and S. DEI POLI, Finite element studies of shear critical R/C beams, Journal of the Engineering Mechanics Division, EM 3, June 1977, pp. 395-410.
11. CERVENKA, V., Inelastic finite element analysis of reinforced concrete panels under in-plane loads, Doctor Thesis, University of Colorado, 1970.
12. CHUNG, H. W., Shear strength of concrete joints under dynamic loads, Concrete, March 1978, pp. 27-29.
13. COLLEY, B. E. and H. A. HUMPHREY, Aggregate interlock at joints in concrete pavements, Highway Research Record, No. 189, 1967, pp. 1-18.
14. COWAN, J. and A. F. CRUDEN, Second thoughts on shear friction, Concrete, August 1975, pp. 31-32.
15. DULACKSKA, H., Dowel action of reinforcement crossing cracks in concrete, ACI-Journal, Vol. 69, No. 12, Dec. 1972, pp. 754-757 (Digest Paper + Supplement).
16. EBBINGHAUS, P., Herleitung eines Verfahrens zur Berechnung von Stahlbeton unter Berücksichtigung der Rissentwicklung, Dissertation, RWTH Aachen, 1975.
17. EIBL, J. and G. IVANYI, Studie zum Trag- und Verformungsverhalten von Stahlbeton, Deutscher Ausschuss für Stahlbeton, Heft 260, Berlin 1976, pp. 200-217.
18. ELEIOTT, A. F., An experimental investigation of shear transfer across cracks in reinforced concrete, M.S. Thesis, Cornell University, Ithaca, June 1974.
19. FATTAH SHAIK, A., Proposed revisions to shear friction provisions, PCI-Journal, March/April 1978, pp. 12-21.
20. FENWICK, R. C. and T. PAULAY, Mechanisms of shear resistance of concrete beams, Journal of the Structural Division, ASCE, Vol. 94, No. ST 10, Proc. Paper 2325, Oct. 1968, pp. 2325-2350.
21. FINNEY, E., Structural design considerations for pavements joints, ACI-Journal, Proceedings, Vol. 53, No. 1, 1956, pp. 17-30.
22. FINNEY, E. A. and W. O. FREMONT, Progress report on load deflection tests dealing with length and size of dowels, Proceedings, Highway Research Board, V 27, 1947, p. 171.
23. FORSELL, C., Schubfestigkeit und Schubbewehrung der Betonbalken, Transactions of the Royal Institute of Technology, No. 78, Stockholm 1954.
24. FRANKLIN, H. A., Non-linear analysis of reinforced concrete frames and panels, Dissertation, University of California, Berkeley, 1970.
25. FRIBERG, B. F., Load and deflection characteristics of dowels in transverse joints of concrete pavements, Highway Research Board, Proceedings, Vol. 18, Part I, 1940, pp. 154-173.

26. FRIBERG, B. F., Design of dowels in transverse joints of concrete pavements, Transactions, ASCE, Vol. 105, 1940, pp. 1078-1080.
27. GEISTEFELD, H., Stahlbetonscheiben in gerissenem Zustand - Berechnung mit Berücksichtigung der rissabhängigen Schubsteifigkeit im Materialgesetz, Dissertation, T.U. Braunschweig 1976.
28. GERGELY, P., J. F. STANTON and R. N. WHITE, Behaviour of cracked concrete nuclear containment vessels during earthquakes, U.S. National Conference on earthquake engineering, University of Michigan, June 1975, pp. 512-518.
29. GOTO, Y., Cracks formed in concrete around deformed tension bars, ACI-Journal, Proceedings, Vol. 68, No. 4, April 1971, pp. 244-251.
30. GRINTER, L. E., Design of reinforced concrete road slabs, Texas Engineering Experimental Station Bulletin, No. 39, Texas 1931.
31. HAND, F. R., D. A. PECKNOLD and W. C. SCHNOBRICH, Non-linear layered analysis of RC plates and shells, Journal of the Structural Division, ASCE, Vol. 99, No. ST 7, Proc. Paper 9860, July 1973.
32. HERMANSEN, B. R. and J. COWAN, Modified shear-friction theory for bracket design, ACI-Journal, No. 2, Febr. 1974, pp. 55-60.
33. HOFBECK, J. A., I. O. IBRAHIM and A. H. MATTOCK, Shear transfer in reinforced concrete, ACI-Journal, Vol. 66, No. 2, Febr. 1969, pp. 119-128.
34. HOUDE, J. and M. S. MIRZA, A finite element analysis of shear strength of reinforced concrete beams, ACI-Special Publication Shear in reinforced concrete, SP-42, Vol. I, pp. 103-128.
35. ISENBERG, J. and S. ADHAM, Analysis of orthotropic reinforced concrete structures, Journal of the Structural Division, Proceedings of the ASCE, Vol. 96, ST 12, Dec. 1970, pp. 2607-2624.
36. JIMENEZ, R., P. PERDIKARIS, P. GERGELY and R. N. WHITE, Interface shear transfer and dowel action in cracked reinforced concrete subject to cyclic shear, Methods of Structural Analysis, Proceedings of the ASCE Conference, Madison, August 1976, pp. 457-475.
37. JIMENEZ, R., Shear transfer across cracks in reinforced concrete, Ph.D. Thesis, Cornell University, 1979.
38. JOHNSTON, D. W. and P. ZIA, Analysis of dowel action, Journal of the Structural Division, ASCE, St 5, May 1971.
39. JONES, R., The ultimate strength of reinforced concrete beams in shear, Magazine of concrete Research, Vol. 8, No. 23, Aug. 1956, pp. 69-84.
40. KLEIN, D., R. KRISTJANSSON, J. LINK, G. MEHLHORN and H. SCHAEFER, Zur Berechnung von dünnen Stahlbetonplatten bei Berücksichtigung eines wirklichkeitsnahen Wekstoffverhaltens, Forschungsbericht No. 25, Institut für Massivbau, T.U. Darmstadt, 1975, pp. 1-28.
41. KREFELD, W. and C. W. THURSTON, Contribution of longitudinal steel to shear resistance of reinforced concrete beams, ACI-Journal, Proc. Vol. 63, March 1966, pp. 325-344.
42. KRISHNAMOORTHY, C. S. and A. PANEERSELVAM, A finite element model for non-linear analysis of reinforced concrete framed structures, The Structural Engineer, Aug. 1977, No. 8, Vol. 55.
43. LAIBLE, J. P., R. N. WHITE and P. GERGELY, Experimental investigation of seismic shear transfer across cracks in concrete nuclear containment vessels, ACI-Special Publication SP-53-9, pp. 203-226.
44. LEONHARDT, F., Vorlesungen über Massivbau, Viertel Teil, Nachweis der Gebrauchsfähigkeit, Springer Verlag, Berlin, Heidelberg, New York 1976.
45. LIN, C. S. and A. C. SCORDELIS, Non-linear analysis of RC shells of general form, Journal of the Structural Division, ASCE, ST 3, March 1975, pp. 523-537.
46. LOE, J. A., Dowel bar joints for airfield pavements, Journal of Institution of Civil Engineers, London, Vol. 1, Oct. 1952, p. 625.
47. LOOV, R., The determination of stresses and deformations of reinforced concrete after cracking, Proceedings of the Southampton 1969 Civ. Eng. Materials Conference, pp. 1257-1260.
48. LORENTSEN, M., Shear and bond in prestressed concrete beams without shear reinforce-

- ment, Transactions of the Royal Institute of Technology, No. 47, Stockholm 1964.
49. MARCUS, H., Load carrying capacity of dowels at transverse pavement joints, Proceedings, ACI-Journal, Vol. 23, Oct. 1951, pp. 169-184.
  50. MAST, R. F., Auxiliary reinforcement in concrete connections, Journal of the Structural Division, ASCE, Vol. 94, ST6, June 1968, pp. 1485-1504.
  51. MATTOCK, A. H. and N. M. HAWKINS, Research on shear transfer in reinforced concrete, PCI-Journal, Vol. 2, March/April 1972, pp. 55-75.
  52. MATTOCK, A. H., Shear transfer in concrete having reinforcement at an angle to the shear plane, ACI-Special Publication SP-42 Shear in reinforced concrete, Vol. I, pp. 17-42.
  53. MATTOCK, A. H., Effect of aggregate type on single direction shear transfer strength in monolithic concrete, Report SM 74-2, Department of Civil Engineering, University of Washington, Seattle, Washington, Aug. 1974.
  54. MATTOCK, A. H., Effect of moment and tension across the shear plane on single direction shear transfer strength in monolithic concrete, Report SM 74-3, Department of Civil Engineering, University of Washington, Seattle, Washington, August 1974.
  55. MATTOCK, A. H., L. JOHAL and H. C. CHOW, Shear transfer in reinforced concrete with moment or tension acting across the shear plane, PCI-Journal, July/Aug. 1975.
  56. MATTOCK, A. H., W. K. LI and T. C. WANG, Shear transfer in lightweight reinforced concrete, Journal of the Prestressed Concrete Institute, Vol. 21, Jan./Febr. 1976, pp. 20-39.
  57. MILLS, G. M., A partial kinking yield criterion for reinforced concrete slabs, Magazine of Concrete Research, Vol. 27, No. 90, March 1975, pp. 13-22.
  58. MUELLER, P., Failure mechanisms for reinforced concrete beams in torsion and bending, Bericht Nr. 65, Institut für Baustatik und Konstruktion, ETH-Zürich, Sept. 1976.
  59. MUELLER, P., Plastische Berechnung von Stahlbetonscheiben und -Balken, Bericht Nr. 83, Institut für Baustatik und Konstruktion, ETH-Zürich, July 1978.
  60. Ngo, D. and A. C. SCORDELIS, Finite element analysis of reinforced concrete beams, ACI-Journal, Vol. 64, No. 3, March 1967, pp. 152-163.
  61. NIELSEN, M. P. and M. W. BRAESTRUP, Plastic shear strength of reinforced concrete beams, Report No. R 73, Structural Research Laboratory, Technical University of Denmark, 1976.
  62. NILSON, A. H., Non-linear analysis of reinforced concrete by the finite element method, ACI-Journal, Sept. 1968, pp. 757-766.
  63. PARK, R. and T. PAULAY, Reinforced concrete structures, Wiley-Interscience Publication, New York, 1975, pp. 319-338.
  64. PAULAY, T., R. PARK and M. H. PHILLIPS, Horizontal construction joints in cast in place reinforced concrete, ACI-Special Publication SP-42 Shear in reinforced concrete, Vol. II, pp. 599-616, 1974.
  65. PAULAY, T. and P. J. LOEBER, Shear transfer by aggregate interlock, ACI-Special Publication SP-42 Shear in reinforced concrete, 1974, Vol. I, pp. 1-16.
  66. PCI - Design Handbook, Prestressed Concrete Institute, Chicago, Illinois, 1974.
  67. RASMUSSEN, B. H., Strength of transversely loaded bolts and dowels cast into concrete, Laboratoriet for Bygningastatik, Den. Tecn. Høskole, Meddelelse, Vol. 34, No. 2, 1962.
  68. RATHS, C. H., Discussion of the paper Design proposals for reinforced concrete corbels by A. H. Mattock, PCI-Journal, Vol. 22, No. 2, March/April 1977, pp. 93-98.
  69. SCHAEFER, H., Zur Berechnung von Stahlbetonplatten, Dissertation T.H. Darmstadt, 1976.
  70. SCHIMMELPFENNIG, K., Bruch sicherheitsberechnung von Stahlbeton-Druckbehältern, Deutscher Ausschuss für Stahlbeton, Heft 257, Berlin 1976.
  71. STANTON, J. F., An investigation of dowel action of the reinforcement of nuclear containment vessels and their non-linear dynamic response to earthquake loads, M.S. Thesis, Cornell University, January 1977.
  72. STAUDER, W., Ein Beitrag zur Untersuchung von Stahlbetonscheiben mit Hilfe finiter Elemente unter Berücksichtigung eines wirklichkeitsnahen Stoffverhaltens, Dissertation T.H. Darmstadt, 1976.
  73. SUIDAN, M. and W. C. SCHNOBRICH, Finite element analysis of reinforced concrete, Journal of the Structural Division, Proceedings of the ASCE, Vol. 99, No. ST 10, Oct. 1973, pp. 2109-2122.

74. SWAMY, R. N. and A. D. ANDRIOPOULOS, Contribution of aggregate interlock and dowel forces to the shear resistance of reinforced beams with web reinforcement, ACI-Special Publication SP-42, 1974, Vol. I, pp. 129-166.
75. SWOBODA, G., Rissuntersuchungen in Stahlbetonbalken und Scheiben mit Hilfe des L.S.T.-Element, Der Bauingenieur, Vol. 50, 1975, No. 12, pp. 465-468.
76. TASSIOS, T. P. and E. VINTZELAEU, Shear force - displacement characteristics of prestressed connections, Proceedings of the RILEM-CEB-CIB Symposium on mechanical and insulating properties of joint of precast reinforced concrete elements, Vol. 1, Athens, Sept. 1978.
77. TAYLOR, H. P. J., Investigation of the forces across cracks in reinforced concrete beams in shear by aggregate interlock, Technical Report No. 42.447, Cement and Concrete Association, November 1970.
78. TAYLOR, H. P. J., Fundamental behaviour in bending and shear of reinforced concrete, Thesis, London, 1971.
79. TAYLOR, H. P. J., The fundamental behaviour of reinforced concrete beams in bending and shear, ACI-Special Publication SP-42 Shear in reinforced concrete, 1974, Vol. I, pp. 43-78.
80. TELLER, L. W. and H. D. CASHELL, Performance of dowelled joints under repetitive loading, Public Roads, Journal of Highway Research. Bureau of Public Roads, U.S. Department of Commerce, Washington, D.C., April 1958.
81. TELLER, L. W. and E. J. SUTHERLAND, A study of structural action of several types of transverse and longitudinal joint design, Public Roads, Vol. 17, No. 7, Sept. 1936.
82. THUERLIMANN, B., Shear strength of reinforced and prestressed concrete beams - CEB Approach, and Torsional strength of reinforced and prestressed concrete beams - CEB Approach, Lecture, ACI Symposium Philadelphia, 1976.
83. TIMOSHENKO, S. and J. M. LESSELS, Applied elasticity, Westinghouse Technical Night School Press, East Pittsburg, Pa., 1925.
84. VANGSIRIRUNGRUANG, K., Effect of normal compressive stresses on shear transfer in reinforced concrete, MSCE Thesis, University of Washington, Seattle, July 1971.
85. WALRAVEN, J. C., The influence of depth on the shear strength of lightweight concrete beams without shear reinforcement, Report No. 5-78-4, May 1978, Stevin Laboratory, Delft, University of Technology, Holland.
86. WEAVER, J. and A. J. CLARK, The effect of dowel bar misalignment in the joints of concrete roads, Technical Report 42.448, Cement and Concrete Association, Nov. 1970.
87. WHITE, R. N. and M. J. HOLLEY, Experimental studies of membrane shear transfer, Journal of the Structural Division, ASCE, Aug. 1972, pp. 1835-1665 and Discussions: July 1973, pp. 1664-1665 and April, pp. 816-818.
88. WHITE, R. N. and P. GERGELEY, Final report on shear transfer in thick walled reinforced concrete structures under seismic loading, Report 78-2, Department of Structural Engineering, Cornell University, Ithaca, New York, May 1978.
89. YUZUGULLU, O. and W. C. SCHNOBRICH, A numerical procedure for the determination of the behaviour of a shear wall frame system, ACI-Journal, Proceedings, Vol. 70, No. 7, July 1973, pp. 474-479.
90. ZIENKIEWICS, O. C., S. VALLIAPAN and I. P. KING, Stress analysis of rock as "no-tension" material, Geotechnique, Vol. 18, 1968, pp. 56-66.
91. ZIENKIEWICS, O. C., D. V. PHILLIPS and P. R. J. OWEN, Finite element analysis of some concrete non-linearities - Theory and examples. Proceedings of the Seminar Concrete Structures subjected to triaxial stresses, May 1974, Bergamo, Italy.
92. WALRAVEN, J. C., Mechanisms of shear transfer in cracks in concrete. A survey of literature. Stevin report 5-78-12, Delft University of Technology, Delft 1978.
93. WALRAVEN, J. C., E. VOS and H. W. REINHARDT, Experiments on shear transfer in cracks in concrete. Part I: Description of results. Stevin report 5-79-3, Delft University of Technology, Delft 1979.
94. WALRAVEN, J. C., Aggregate interlock - a theoretical and experimental analysis, Thesis, Delft University of Technology, October 1980, The Netherlands.
95. REHM, G., Über die Grundlagen des Verbundes zwischen Stahl und Beton, DAfStb, Heft 138, Berlin 1961.

96. WEISS, R., Ein haufwerkstheoretisches Model der Restfestigkeit geschädigter Betone, Dissertation, T.U. Braunschweig 1978, pp. 37-47.
97. MARTIN, H., Zusammenhang zwischen Oberflächenbeschaffenheit, Verbund und Sprengwirkung von Bewehrungsstählen unter Kurzzeitbelastung, Deutscher Ausschuss für Stahlbeton, Heft 228, Berlin 1973.
98. BAZANT, Z. P. and P. GAMBAROVA, Rough cracks in reinforced concrete, Journal of the Structural Division, Proc. ASCE, Vol. 106, 1980, pp. 819-842.
99. GAMBAROVA, P., Shear transfer by aggregate interlock in cracked reinforced concrete subject to repeated loads, Studi e Recherche, Vol. 1, 1979, Politecnico di Milano, Italy.
100. FARDIS, M. and O. BUYUKOZTURK, Shear transfer model for reinforced concrete, Journal of the Engineering Mechanics Division, Proc. ASCE, April 1979, pp. 255-275.
101. FARDIS, M. and O. BUYUKOZTURK, Shear stiffness of concrete by Finite Elements, Journal of the Structural Division, Proc. ASCE, June 1980, pp. 1311-1327.
102. WHITE, R. N., P. C. PERDICARIS and P. GERGELEY, Strength and stiffness of reinforced concrete containments, subjected to seismic loading: research results and needs, Nuclear Conference, Berlin, Aug. 1979.
103. BROMS, B. B., Crack width and crack spacing in reinforced concrete members, ACI-Journal, Proc. Vol. 62, No. 10, Oct. 1965, pp. 1237-1256.
104. BROMS, B. B., Stress distribution in reinforced concrete members with tension cracks, ACI-Journal, Proc. Vol. 62, No. 9, Sept. 1965, p. 1095.
105. BROMS, B. B., Techniques for investigation of internal cracks in reinforced concrete members, ACI-Journal, Jan. 1965, pp. 35-44.
106. BROMS, B. B., and L. A. LUTZ, Effects of arrangement of reinforcement on crack width and spacing of reinforced concrete members, ACI-Journal, Nov. 1965, pp. 1395-1410.
107. BASE, B. D., J. B. READ, A. W. BEEBY and H. P. J. TAYLOR, An investigation of the crack control characteristics of various types of bar in reinforced concrete beams, C&CA Research Report 18, Dec. 1966.
108. BEEBY, A. W., A study of cracking in reinforced concrete members subjected to pure tension, Technical Report No. 42.468, C&CA, London, 1972.
109. REHM, G. and H. MARTIN, Zur Frage der Rissbegrenzung im Stahlbetonbau, 8/1968, pp. 175-182.
110. MONTERIO, General theory of cracking, CEB-Bulletin d'Information 89, March 1973.
111. FERRY-BORGES, J., Cracking and deformability of reinforced concrete beams, IABSE, Vol. 26, 1966.
112. EFSEN, A., Tensile cracks in reinforced concrete, Ingenieur 71e Jaargang, No. 41, Okt. 1959.
113. BEEBY, A. W., The prediction of crack widths in hardened concrete, The Structural Engineer, Vol. 57A, No. 1, Jan. 1979.
114. ROSTASY, F. and W. ALDA, Rissbreitenbeschränkung bei zentrischem Zwang von Stäben aus Stahlbeton und Stahlleichtbeton, Beton- und Stahlbetonbau, 6/1977, pp. 149-156.
115. FALKNER, H., Zur Frage der Rissbildung durch Eigen- und Zwangspannungen infolge Temperatur in Stahlbetonbauteilen, Deutscher Ausschuss für Stahlbeton, Heft 208, Berlin.
116. ROSTASY, F., R. KOCH and F. LEONHARDT, Zur Mindestbewehrung für Zwang von Außenwänden aus Stahlleichtbeton, Deutscher Ausschuss für Stahlbeton, Heft 267.
117. LEONHARDT, F., Vorlesungen über Massivbau, Vierter Teil, Nachweis der Gebrauchsfähigkeit, Dictaat TH Stuttgart, 1976.
118. STRANINGER, W., Einfluss einer Langzeitbelastung auf die Spannungs-Dehnungslinie, 11-er Forschungskolloquium des Deutschen Ausschusses für Stahlbeton, Kurzfassung der Referate, Universität Innsbruck, März 1980.
119. CEB Model Code for Concrete Structures, 1978.
120. CLARK, A. P., Cracking in reinforced concrete flexural members, ACI-Journal, April 1965, pp. 851-862.
121. KAAR, P. H. and A. H. MATTOCK, High strength bars as concrete reinforcement - control of cracking, PCI-Journal, Jan. 1963, pp. 15-38.
122. PETER, J., Zur Bewehrung von Scheiben un Schalen für Hauptspannungen schiefwinklig zur Bewehrungsrichtung, Dissertatie TH Stuttgart, 1964.

## 12 Appendices

### 12.1 Composition of the concrete mixtures used in the experiments

Mix 1	concrete composition		grading of aggregate	
	components	kg/m <sup>3</sup>	particle size mm	mass kg
	aggregate <sup>1</sup>	1950	8-16	613
	cement B <sup>2</sup>	250	4-8	433
	water	156	2-4	307
	quartz powder	50	1-2	217
	total	2406	0.5-1	153
			0.25-0.5	108
	strength $f_{cc} = 29.5 \text{ N/mm}^2$		< 0.25	119
			total	1950
Mix 2	concrete composition		grading of aggregate	
	components	kg/m <sup>3</sup>	particle size mm	mass kg
	aggregate	1944	8-16	715
	cement B	250	4-8	506
	water	156	2-4	358
	quartz powder	50	1-2	253
	total	2400	0.5-1	-
			0.25-0.5	-
	strength $f_{cc} = 29.5 \text{ N/mm}^2$		< 0.25	112
			total	1944
Mix 3	concrete composition		grading of aggregate	
	components	kg/m <sup>3</sup>	particle size mm	mass kg
	aggregate	1878	8-16	702
	cement B	400	4-8	378
	water	160	2-4	306
	totaal	2438	1-2	224
			0.5-1	114
	strength $f_{cc} = 56.1 \text{ N/mm}^2$		0.25-0.5	136
			< 0.25	18
			total	1878

<sup>1</sup> rounded, glacial river aggregate

<sup>2</sup> Portland cement, type B (according to Dutch Standard)

Mix 4

concrete composition

components	kg/m <sup>3</sup>
aggregate	1830
cement B	195
water	165
quartz powder	143
total	2323

strength  $f_{cc} = 19.9 \text{ N/mm}^2$

grading of aggregate

particle size mm	mass kg
8-16	682
4-8	378
2-4	296
1-2	215
0.5-1	113
0.25-0.5	135
< 0.25	11
total	1830

Mix 5

concrete composition

components	kg/m <sup>3</sup>
aggregate	2033
cement B	209
water	104
quartz powder	34
total	2380

strength  $f_{cc} = 38.2 \text{ N/mm}^2$

grading of aggregate

particle size mm	mass kg
16-32	598
8-16	507
4-8	227
2-4	80
1-2	106
0.5-1	219
0.25-0.5	262
< 0.25	34
totaal	2033

Mix 6

concrete composition

components	kg/m <sup>3</sup>
Korlin A <sup>1</sup>	570
sand	681
cement B	353
water	140
total	1744

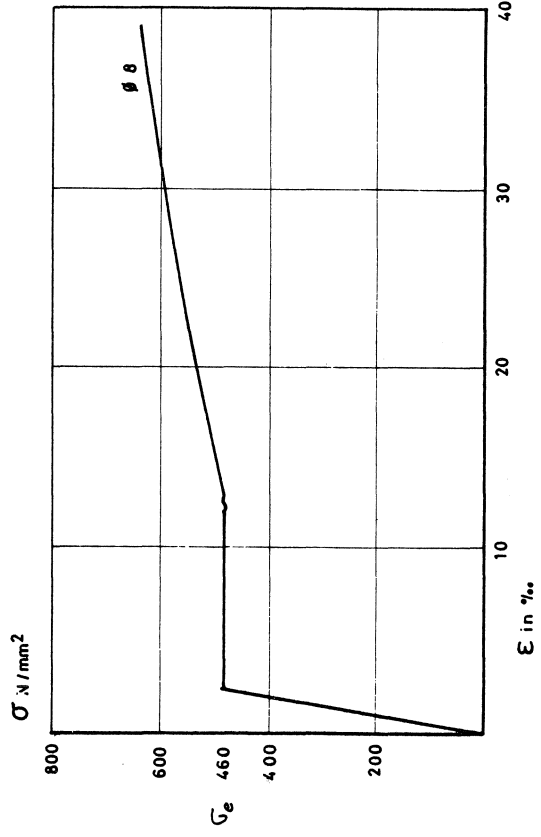
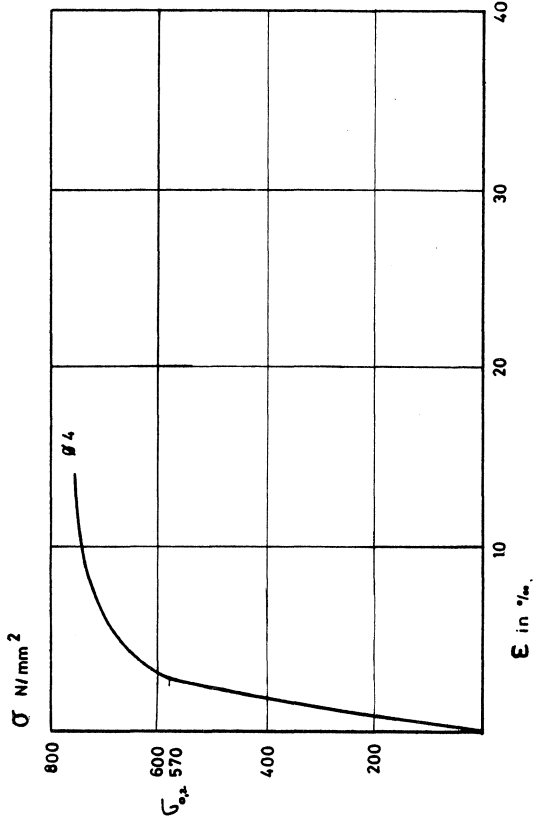
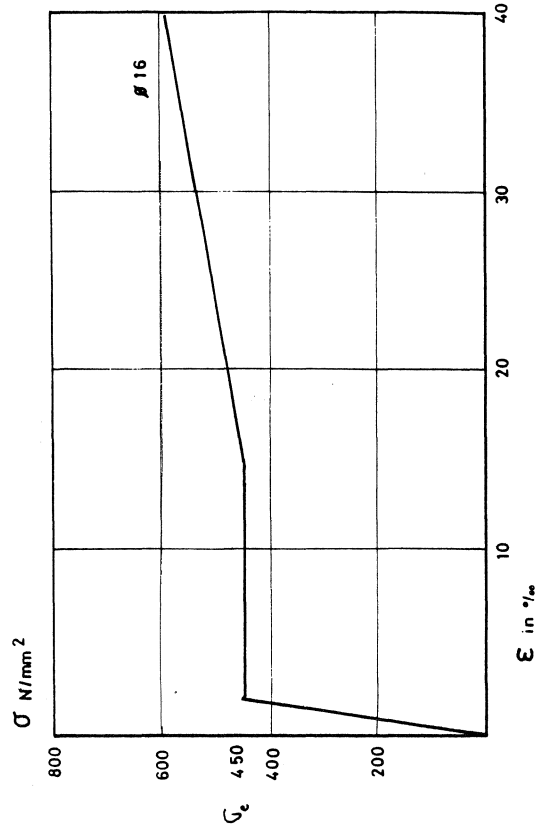
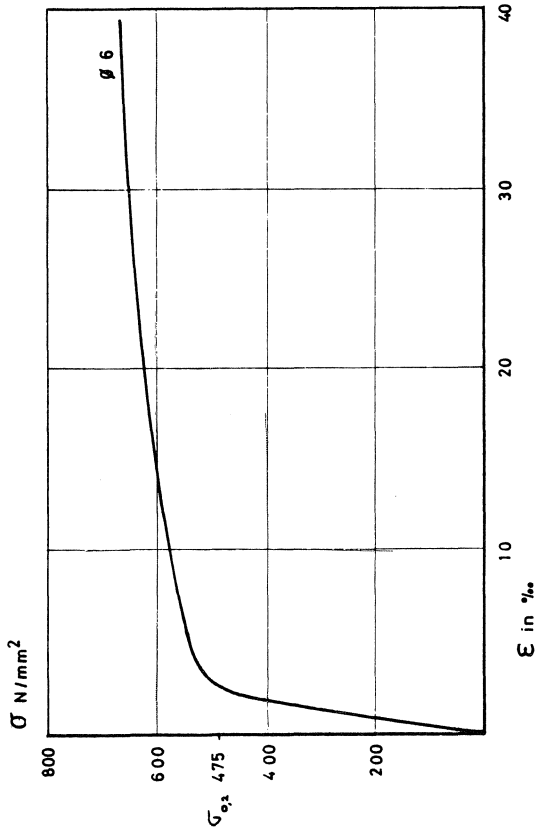
strength  $f_{cc} = 38.1 \text{ N/mm}^2$

grading of aggregate

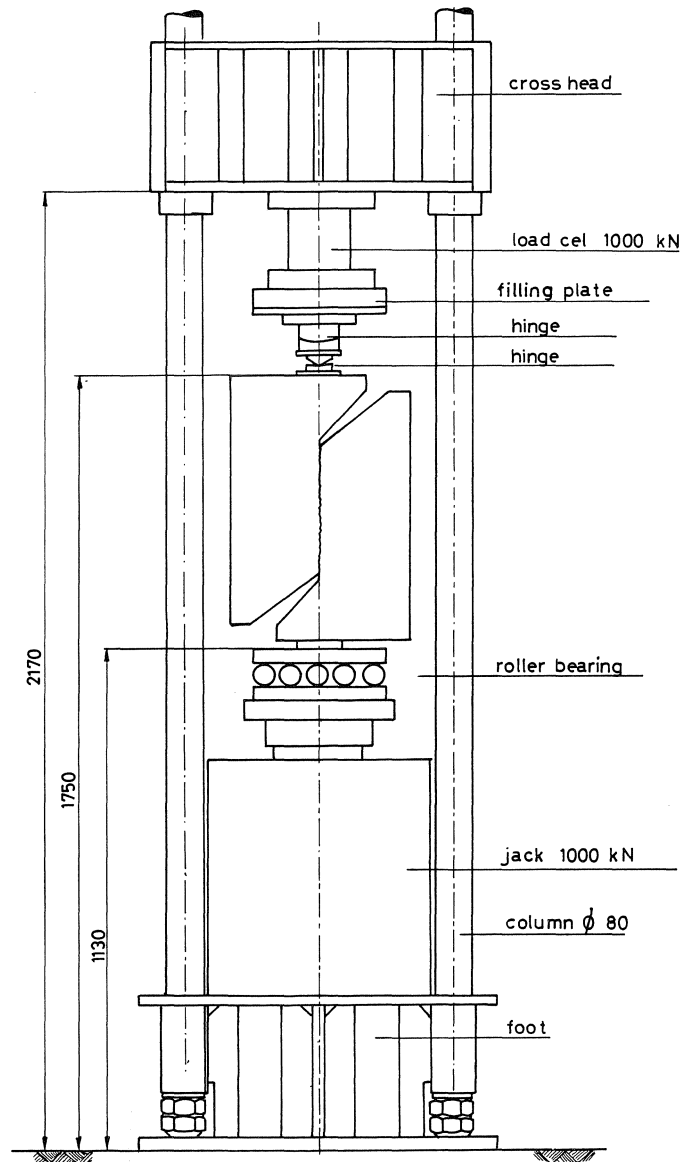
particle size mm	mass kg
4-8	17
2-4	222
1-2	171
0.5-1	84
0.25-0.50	143
< 0.25	44
total	681

<sup>1</sup> expanded clay

12.2 Stress-strain diagram of the stirrup reinforcing steel



12.3 Loading arrangement used for the tests



## 12.4 Tests on specimens with embedded bars

### 12.4.1 Reinforcement normal to the crack

type of aggregate	code	reinf. ratio (%)	$\rho f_c$ (N/mm <sup>2</sup> )	amount of stirr.	diam. stirr. (mm)	mix	in.crack width (mm)	cube strength (N/mm <sup>2</sup> )	splitt. strength (N/mm <sup>2</sup> )	ult.shear strength (N/mm <sup>2</sup> )	remarks
gravel	110208t	0.56	2.43	2	8	1	0.03	35.9	2.4	5.08	
$D_{\max} = 16$	110208	0.56	2.43	2	8	1	0.02	30.7	2.4	5.50	
	110208g	0.56	2.43	2	8	1	0.09	29.4	2.2	5.08	
	110408	1.12	4.86	4	8	1	0.03	30.7	2.4	6.44	second loading after 4 months*
	110608	1.68	7.29	6	8	1	0.01	30.7	2.4	7.39	
	110808t	2.23	9.72	8	8	1	0.05	35.9	2.4	7.78	initial loading rate too high
	110808	2.23	9.72	8	8	1	0.02	30.7	2.4	7.08	failure by secondary cracks
	110808h	2.23	9.72	8	8	1	0.01	29.4	2.2	8.39	
	110808hg	2.23	9.72	8	8	1	0.07	29.4	2.2	8.58	
	110706	1.10	5.58	7	6	1	0.02	31.7	2.5	7.19	second loading after 5 months*
	210204	0.14	1.06	2	4	1	0.08	36.6	2.8	3.22	
210608	1.68	7.29	6	8	1	0.00	36.6	2.8	9.72		
210216	2.23	10.12	2	16	1	0.02	36.6	2.8	9.25		
210316	3.35	15.17	3	16	1	0.02	36.6	2.8	10.11		
210808h	2.23	9.72	8	8	1	0.02	25.2	1.7	7.97	concrete strength too low by malfunction of climate room	
gravel	120208	0.56	2.43	2	8	2	0.04	29.5	2.1	5.36	second loading after 5 months*
$D_{\max} = 16$	120408	1.12	4.86	4	8	2	0.04	29.5	2.1*	6.53	second loading after 5 months*
	120608	1.68	7.29	6	8	2	0.01	29.5	2.1	6.78	
discont. grading	120808	2.23	9.72	8	8	2	0.02	29.5	2.1	7.31	
	120706	1.10	5.58	7	6	2	0.02	29.2	2.2	6.92	second loading after 5 months*
	120216	2.23	10.12	2	16	2	0.03	29.2	2.2	6.53	
gravel	230208	0.56	2.43	2	8	3	0.05	56.1	4.0	6.72	
$D_{\max} = 16$	230408	1.12	4.86	4	8	3	0.02	56.1	4.0	10.83	
	230608	1.68	7.29	6	8	3	0.03	56.1	4.0	12.56	
	230808	2.23	9.72	8	8	3	0.02	56.1	4.0	14.19	
gravel	240208	0.56	2.43	2	8	4	0.01	19.9	1.4	4.65	
$D_{\max} = 16$	240408	1.12	4.86	4	8	4	0.01	19.9	1.4	6.04	
	240608	1.68	7.29	6	8	4	0.01	19.9	1.4	6.55	
	240808	2.23	9.72	8	8	4	0.01	19.9	1.4	6.29	
gravel	250208	0.56	2.43	2	8	5	0.01	38.2	3.0	6.83	
$D_{\max} = 32$	250408	1.12	4.86	4	8	5	0.01	38.2	3.0	8.69	
	250608	1.68	7.29	6	8	5	0.01	38.2	3.0	9.65	
	250808	2.23	9.72	8	8	5	0.01	38.2	3.0	9.94	
light-weight (Korlin)	260208	0.56	2.43	2	8	6	0.01	34.4	2.9	6.52	results influenced by malfunction of the top hinge
	260408	1.12	4.86	4	8	6	0.01	34.4	2.9	8.62	
	260608	1.68	7.29	6	8	6	0.01	34.4	2.9	9.79	
	260808	2.23	9.72	8	8	6	0.01	34.4	2.9	10.36	
	260208h	0.56	2.43	2	8	6	0.04	38.1	2.5	4.09	
	260808h	2.23	9.72	8	8	6	0.02	38.1	2.5	8.87	
	310208	0.56	2.43	2	8	1	0.04	36.1	-	5.95	soft sleeves around rebars
	310408	1.12	4.86	4	8	1	0.02	36.1	-	8.15	20 mm to both sides of the crack
	310608	1.68	7.29	6	8	1	0.02	36.1	-	8.81	
	310808	2.23	9.72	8	8	1	0.01	36.1	-	8.94	

\* only the  $\tau_c$ -values for the first loading are presented

## 12.4.2 Reinforcement inclined to the crack plane

type of aggregate	code	reinf. ratio (%)	$\rho f_c$ (N/mm <sup>2</sup> )	amount of stirr.	diam. stirr. (mm)	angle with crack plane	mix	in.crack width (mm)	cube strength (N/mm <sup>2</sup> )	splitt. strength (N/mm <sup>2</sup> )	ult.shear strength (N/mm <sup>2</sup> )	remarks
gravel	21.045	0.56	2.43	2	8	45°	1	0.06	34.2	2.97	6.97	
$D_{\max} = 16$	21.068	0.56	2.43	2	8	67.5°	1	0.02	34.2	2.97	6.83	
	21.112	0.56	2.43	2	8	112.5°	1	0.02	34.2	2.97	4.81	
	21.135	0.56	2.43	2	8	135°	1	0.05	34.2	2.97	2.92	
	21.060	0.56	2.43	2	8	60°	1	0.01	37.6	2.64	7.59	results influenced by malfunction of top hinge
	21.075	0.56	2.43	2	8	75°	1	0.01	37.6	2.64	7.25	
	21.105	0.56	2.43	2	8	105°	1	0.01	37.6	2.64	5.96	
	21.120	0.56	2.43	2	8	120°	1	0.01	37.6	2.64	4.46	

## 12.5 Tests on specimens with external bars

type of aggregate	code	restr. stress at $w=0.6$ mm (N/mm <sup>2</sup> )	initial crack width (mm)	initial shear displ. (N/mm <sup>2</sup> )	cube crushing strength (N/mm <sup>2</sup> )	cube splitting strength (N/mm <sup>2</sup> )
gravel	1/0/3.6	3.6	0.03	0.00	36.7	2.6
$D_{\max} = 16$ mm	1/0/7.8	7.8	0.01	0.00	38.5	2.8
	1/2/ .4	0.4	0.23	0.04	36.7	2.6
	1/2/1.4	1.4	0.19	0.04	36.7	2.6
	1/2/1.6	1.6	0.18	0.04	38.5	2.8
	1/4/ .3	0.3	0.41	0.02	38.5	2.8
	1/4/1.0	1.0	0.40	0.06	38.5	2.8
	1/0/5.4	5.4	0.01	0.00	25.2	1.7
	1/2/ .2	0.2	0.20	0.02	25.2	1.7
	1/4/ .4	0.4	0.39	0.03	25.2	1.7
gravel	3/0/5.1	5.1	0.02	0.00	57.4	4.0
$D_{\max} = 16$ mm	3/0/6.2	6.2	0.02	0.00	60.8	3.8
	3/0/6.9	6.9	0.02	0.00	60.8	3.8
	3/0/7.5	7.5	0.02	0.00	57.4	4.0
	3/2/1.7a	1.7	0.20	0.00	60.8	3.8
	3/2/1.7b	1.7	0.20	0.04	57.4	4.0
	3/4/ .6	0.6	0.40	0.06	57.4	4.0
	3/4/1.9	1.9	0.41	0.08	60.8	3.8
gravel	4/0/4.0	4.0	0.02	0.00	13.4	1.4
$D_{\max} = 16$ mm	4/0/4.2	4.2	0.03	0.00	13.4	1.4
	4/2/2.0	2.0	0.20	0.00	13.4	1.4
	4/4/0.8	0.8	0.38	0.06	13.4	1.4
gravel	5/0/4.9	4.9	0.01	0.00	33.4	2.3
$D_{\max} = 32$ mm	5/0/5.6	5.6	0.02	0.00	33.4	2.3
	5/2/1.8	1.8	0.20	0.02	33.4	2.3
	5/4/1.1	1.1	0.40	0.05	33.4	2.3
light-weight aggregate	6/0/4.4	4.4	0.02	0.00	39.3	2.5
	6/0/5.4	5.4	0.02	0.00	39.3	2.5
	6/2/2.4	2.4	0.20	0.06	39.3	2.5
Korlin A	6/2/ .4	0.4	0.19	0.03	38.1	2.5
	6/4/ .7	0.7	0.39	0.06	39.3	2.5
	6/4/ .3	0.3	0.40	0.14	38.1	2.5